Check for updates

Received: 19 December 2024 | Revised: 21 August 2025 | Accepted: 30 August 2025

DOI: 10.1002/esp.70159

RESEARCH ARTICLE

ESPL WILEY

Time scales of river bifurcations

Gabriele Barile[1] | Marco Redolfi[2] | Marco Tubino[1]

[1]Department of Civil, Environmental and Mechanical Engineering, University of Trento, Trento, Italy

[2]Department of Engineering "Enzo Ferrari", University of Modena and Reggio Emilia, Modena, Italy

Correspondence
Gabriele Barile, Department of Civil, Environmental and Mechanical Engineering, University of Trento, Trento, Italy.
Email: gabriele.barile@unitn.it

Funding information
This work has been carried out within the projects "SEDMORNET" funded by the European Union Next-GenerationEU (Piano Nazionale di Ripresa e Resilienza PNRR) – Mission 4 - Component C2 - Investment Fund 1.1 "Fondo per il Programma Nazionale di Ricerca e Progetti di Rilevante Interesse Nazionale (PRIN)," and the project DICAM-EXC (Departments of Excellence 2023–2027, grant L232/2016).

Abstract

River bifurcations are the fundamental building blocks of a variety of fluvial environments such as braiding and anastomosed rivers, alluvial fans, and river deltas. Their long-term equilibrium configurations have been widely explored, together with the influence of several external forcing factors, whereas less attention has been devoted to investigate the characteristic timescale with which bifurcations evolve over time. In this work, we address this issue by combining the results of a 1-D numerical model with those obtained through a linear stability analysis that accounts for the length of bifurcates. Numerical results show that the timescale of the adaptation of water and sediment partition at the bifurcation node is much shorter than the time required to achieve the long-term equilibrium of the bifurcates. We find that the nodal point evolution becomes faster as the value of the width-to-depth ratio increases above the critical threshold for the bifurcation stability, while it gets slower as the length of the bifurcates increases. The timescale becomes independent of the branch length when this length exceeds a threshold value above which the effect of the downstream boundary condition no longer affects the evolution of the bifurcation node. The analysis of a large dataset of gravel-bed bifurcations reveals that the evolutionary timescale of most of them is larger than that of natural flow variations. Moreover, the rate at which the water and sediment partitioning at bifurcations changes over time is generally smaller than the fluctuation rate of sediment transport caused by the migration of bars in the upstream channel, especially for bifurcations with long branches.

KEYWORDS
linear analysis, numerical modelling, open channel flow, river bifurcations, river morphodynamics, sediment transport

1 | INTRODUCTION

The evolution of dynamical systems is determined by the combination of various processes acting on different timescales. River systems are no exception, as their evolutionary trajectories are controlled by the relative rates of different morphodynamic processes and by the rate of change of external forcings. Recognizing a hierarchy of time (and spatial) scales is crucial to explain the occurrence of the variety of sedimentary patterns observed in fluvial environments, while it also provides a powerful tool to identify suitable modelling approaches for specific morphodynamical problems (Seminara, 2010). A notable example is the key assumption of instantaneous adaptation of the flow field and bed topography to planform changes, on which theoretical models of the evolutionary trajectories of river meanders are commonly based (Bogoni et al., 2017; Eke et al., 2014; Monegaglia et al., 2019; Seminara et al., 2001).

Jerolmack and Mohrig (2007) provided a straightforward example of the application of scaling analysis to channel branching in depositional rivers, arguing that the relative velocity of bank migration, as compared to that of channel sedimentation, determines whether a river preferably evolves towards a single-thread or a multithread configuration. The ratio between the timescales of bank erosion and

This is an open access article under the terms of the Creative Commons Attribution License, which permits use, distribution and reproduction in any medium, provided the original work is properly cited.
© 2025 The Author(s). *Earth Surface Processes and Landforms* published by John Wiley & Sons Ltd.

riverbed evolution was also found to govern the response of the bankfull geometry of developing meandering reaches (Monegaglia & Tubino, 2019; Parker et al., 2011).

Other studies investigated the role exerted by the variability of external forcings on individual fluvial processes, such as the relationships between the time variability of sediment supply and the avulsion timescale in braided rivers (Ashworth et al., 2004) and the impact of sea-level rise (Chadwick et al., 2020; Liang et al., 2016) and of the hydrological regime (Brooke et al., 2022) on avulsions in alluvial fans and river deltas. In all the mentioned studies, the timescale of the external forcing was scaled with the sediment transport rate, which sets a system-specific reference timescale.

In general terms, this kind of analysis is based on a methodological distinction between the external factors acting at the boundaries and the internal morphodynamic responses, the identification of which depends on the specific process under investigation and on the recognition of their respective timescales. Hence, the definition of the intrinsic timescales of morphodynamic processes is a fundamental prerequisite to determine the capability of external factors to affect the evolutionary trajectories of fluvial systems. This is the case of migrating alternate bars in gravel-bed rivers, as the intrinsic timescale of bar development (i.e., the reciprocal of the bar growth rate) is often comparable with the duration of formative flood events (Tubino, 1991). Building upon this result, Carlin et al. (2021) showed that the dependence on the flow discharge of the intrinsic rate of change of bar amplitude, as obtained from the weakly nonlinear theory of Colombini et al. (1987), plays a crucial role in determining the response of river bars to the hydrological regime and ultimately controls their long-term average characteristics.

Contrary to the aforementioned fluvial environments, the analysis of the characteristic timescale of river bifurcations has received less attention, although their long-term behaviour and equilibrium configurations have been extensively investigated in the last decades. A key feature emerging from field observations is that natural bifurcations are likely to display unbalanced equilibrium configurations, in which one of the two branches carries the larger fraction of the incoming water and sediment discharges (Edmonds & Slingerland, 2008; Kleinhans et al., 2013; Zolezzi et al., 2006). This unbalance often results from the combination of aggradation in the minor branch and erosion in the dominant branch. Clear evidence of this mechanism was provided by the flume experiments of Bertoldi and Tubino (2007), along with several field studies. Among others, the morphodynamic evolution of the bifurcation–confluence unit along the Ain River (France), as reported by Szewczyk et al. (2022), represents a noteworthy example of these processes. Specifically, the recent development of the system features swift variations in the degree of asymmetry of the bifurcation, ranging from quasi-balanced to strongly unbalanced and manifesting an evolutionary timescale of the order of a year (see the sequence of aerial images included in the Supporting Information S1).

As in the case of the Ain River, the aggradation process in the minor branch of bifurcations has often been observed to occur gradually, and specifically in the form of a prograding sediment front, both in laboratory experiments (Szewczyk et al., 2020) and field analyses (Van Denderen et al., 2019). This aggradation process may lead to channel abandonment, which usually manifests itself through the formation of a sediment plug at the branch inlet (e.g., Riquier et al., 2015; Szewczyk et al., 2020; Toonen et al., 2012), resulting in the so-called "choking" avulsion (Ferguson, 1993; Leddy et al., 1993).

The mechanism through which bifurcations develop unbalanced configurations has been widely analysed theoretically by means of the quasi-2D nodal point relation for sediment partitioning originally proposed by Bolla Pittaluga et al. (2003), hereafter referred to as BRT. The main outcome of these analyses is that bifurcations can spontaneously evolve towards unbalanced configurations due to an intrinsic instability mechanism, within a wide range of values of the control parameters (hydraulic geometry and sediment size), even in the absence of external forcings and with a symmetric planform configuration. In real-world bifurcations, such inherent morphodynamic response is likely to be affected by a variety of external forcings, such as alternate bars (Bertoldi et al., 2009; Le et al., 2018), variable water and sediment supply (Mendoza et al., 2022; Miori et al., 2006a), tides (Ragno et al., 2020; Wagner & Mohrig, 2019), prograding branches (Salter et al., 2018), and vegetation growth (Burge, 2006). The influence of these factors on river bifurcations has been studied so far by either focusing on specific case studies or analysing the long-term equilibrium configurations. A key aspect revealed by these studies is that the mark of the intrinsic instability mechanism can also be seen in the equilibrium states of bifurcations subject to nonuniform boundary conditions, such as those determined by a curved upstream reach or by a downstream imposed slope advantage (Redolfi et al., 2019). Thus, while it is known how external factors can compete or cooperate with the intrinsic response of bifurcations to determine their equilibrium states, the time required to achieve these states and the role of these factors in the transient stage still await a quantification.

Previous field observations and numerical analyses have provided some information on the evolutionary timescale of bifurcations. On one hand, the field study of Bertoldi (2012) on a gravel-bed braided reach of the Tagliamento River (Italy) suggested that bifurcations may evolve on a timescale similar to that of bar migration and flood duration. On the other hand, based on field observations in an anabranching river, Burge (2006) argued that the evolutionary timescale of bifurcations depends on the formation mechanism, ranging from swift changes in their morphology for bifurcations formed after neck cutoffs, to slow to no evolution for bifurcations generated by central bars deposition. These observations are suggestive of a dependence of the transient behaviour of bifurcations on the length of the bifurcates, which is known to control the equilibrium states of bifurcation-confluence units (Ragno et al., 2021). Based upon a qualitative analysis of satellite images for four case studies, Van Denderen et al. (2018) suggested that the evolutionary timescales of bifurcations may range from several years up to decades. The authors then coupled their observations with a one-dimensional model, showing how the system timescale can be affected by different forcing factors such as the length ratio of the bifurcates, a curved upstream channel, channel width adaptation, and flow separation at the entrance of the side channel. As for other numerical studies, Delft3D simulations performed by Kleinhans et al. (2008) showed that the evolutionary timescale of bifurcations is of the order of decades, thus much slower than that of "local" morphological changes at the bifurcation node. This result has been recently confirmed by the numerical simulations performed by Gao et al. (2024), who analysed the evolution of an idealized bifurcation subjected to dredging. In their study, the authors pointed out that the rate at which the bifurcation evolved towards its

10969837, 2025, 12, Downloaded from https://onlinelibrary.wiley.com/doi/10.1002/esp.70159 by University Modena, Wiley Online Library on [03/11/2025]. See the Terms and Conditions (https://onlinelibrary.wiley.com/terms-and-conditions) on Wiley Online Library for rules of use; OA articles are governed by the applicable Creative Commons License

equilibrium configuration was very slow, namely of the order of 10^2 times the timescale set by the reference transport capacity (i.e., the Exner timescale).

The above results, although not providing an exhaustive description of the timescale of bifurcations and of its dependence on flow conditions and planform geometry, raise further relevant questions on the matter. How fast is the adaptation of flow and sediment partition at the node, as compared with the time needed to achieve the overall equilibrium of the system? How does the length of the bifurcates affect the speed of this adaptation process? According to the analytical and numerical results obtained using the BRT nodal condition, the equilibrium states of symmetrical bifurcations are independent of the length of the anabranches, provided that both channels are morphodynamically active. However, such states are strongly dependent on the length of the bifurcates when the flow and sediment partition is so unbalanced that one of the two branches ceases to transport sediment (Barile et al., 2024). Whether the length of bifurcates plays a similar role in the transient behaviour of bifurcations remains an open question.

The role of the length of the downstream branches on the evolutionary timescale of bifurcations was first analysed by Miori et al. (2006b). To do so, they used a simplified unsteady model in which the ratio between the channel slopes of the bifurcates was assumed to be constant over time. Therefore, their model was unable to reproduce the effect of local slope changes at the inlets of the distributaries caused by the variation of the water and sediment fluxes delivered by the bifurcation node (i.e., the "boundary layer" effect described for single channels by Wong & Parker, 2006). Local changes in bed slope caused by the uneven partition of water and sediment were also observed in previous numerical simulations of evolving bifurcations (Barile et al., 2024; Kleinhans et al., 2008). Given the sensitivity of equilibrium configurations to an imposed slope advantage (Redolfi et al., 2019), one might expect such local changes to also play a relevant role in the transient behaviour of bifurcations.

In this work, we try to address the questions formulated above by analysing the time evolution of a simple, unforced symmetrical bifurcation. More specifically, we aim at quantifying how the intrinsic timescale of bifurcations depends on the key controlling parameters and on modelling choices. This is accomplished by formulating an unsteady morphodynamic model, based on the quasi-2D nodal point relation of Bolla Pittaluga et al. (2003), in which the full coupling between the node and the downstream channels evolution is retained. This model is then used to analyse the evolution of an initially balanced bifurcation that evolves towards an unbalanced configuration. The governing system of equations is first solved using the fully nonlinear numerical scheme formulated in Barile et al. (2024). Then, the system is analysed through a novel theoretical approach based on a linear, spatially and temporally resolved solution of the model equations.

We analyse model outputs by first providing an operative definition of the intrinsic timescale of bifurcations. Then, we explore its dependence on the governing parameters, namely, the flow conditions in the upstream channel and the length of the bifurcates. Lastly, we compare this timescale with those of some external forcings that most influence the evolution of gravel-bed bifurcations, namely the migration of bars in the upstream channel and the time variability of the flow discharge.

2 | MODEL FORMULATION

We consider a bifurcation composed of three branches having a rectangular cross-section and fixed banks, with the downstream bifurcates having the same length. The system is fed with constant water and sediment supplies, and a fixed water level is imposed at the downstream boundary of the domain. When the sum of the widths of bifurcates equals the upstream channel width, this system admits of a simple steady state solution in which the flow and the sediment transport are uniform in all branches and the bed slope, the depth and the unit water and sediment discharges are identical in the three channels, regardless of the respective widths of bifurcates. We take this equilibrium solution as the initial state of the system, and we then analyse how it evolves in time by applying a small perturbation to the transverse bed slope between the node cells. Without loss of generality, in the following we will assume the widths of the downstream channels to be equal, which implies that water and sediment discharges are split equally between the downstream branches in the initial state. We term the examined configuration "unforced" because the downstream water level is set at the value corresponding to the initial uniform conditions.

To make our problem dimensionless, we scale the variables with the geometric and hydraulic parameters of the reference flow (i.e., the initial uniform flow in the upstream channel), here denoted with the subscript 0. The resulting dimensionless variables read (starred variables refer to dimensional quantities):

$$x := \frac{x^*}{W_0^*/2},\ t := \frac{t^*}{T_E^*},\ (\eta, D) := \frac{(\eta^*, D^*)}{D_0^*},\ U := \frac{U^*}{U_0^*},\ q := \frac{q^*}{q_0^*},\ q_s := \frac{q_s^*}{q_{s0}^*},\ L := \frac{L^*}{D_0^*}, \tag{1}$$

where x^* is the longitudinal coordinate, t^* is time, W^* is the channel width, η^* is the bed elevation, D^* is the flow depth, U^* is the flow velocity, q^* is the flow discharge per unit width, q_s^* is the transport capacity per unit width, and L^* is the length of the bifurcates. The dimensionless time t is defined by scaling t^* with the dimensional timescale T_E^* of the bed evolution defined by the Exner equation

$$T_E^* := (1-p)\frac{W_0^* D_0^*}{2 q_{s0}^*}, \tag{2}$$

where p is the bed porosity.

We compute the unit transport capacity in terms of the local value of the Shields stress θ as

$$q_s^* = \sqrt{\Delta g D_s^3}\,\Phi(\theta),\ \theta = \frac{U^{*2}}{c^2 \Delta g D_s}, \tag{3}$$

where Δ and D_s are the relative submerged density and the grain diameter of sediment particles, respectively, g is gravity, and c is the Chézy coefficient. In the following the latter parameter is assumed to be constant, though the analysis can be readily extended to include its dependence on the local relative roughness. To compute the bedload function Φ, we use the formula proposed by Parker (1978).

The mathematical model is based on the solution of the one-dimensional shallow water flow equations and Exner sediment continuity equation, and adopts a quasi-steady approximation for the

10969837, 2025, 12, Downloaded from https://onlinelibrary.wiley.com/doi/10.1002/esp.70159 by University Modena, Wiley Online Library on [03/11/2025]. See the Terms and Conditions (https://onlinelibrary.wiley.com/terms-and-conditions) on Wiley Online Library for rules of use; OA articles are governed by the applicable Creative Commons License

hydrodynamics. The governing equations can be expressed in dimensionless form as

$$U\frac{\partial U}{\partial x}+\frac{1}{Fr_0^2}\left(\frac{\partial D}{\partial x}-\beta_0 S\right)+\frac{\beta_0 U^2}{c^2 D}=0, \tag{4a}$$

$$\frac{\partial (UD)}{\partial x}=0, \tag{4b}$$

$$\frac{\partial \eta}{\partial t}+\frac{\partial q_s}{\partial x}=0, \tag{4c}$$

where $S=-\partial\eta^*/\partial x^*$ is the local bed slope, Fr_0 is the reference Froude number, and β_0 is the reference half-width to depth ratio (hereafter, aspect ratio).

The formulation of the internal conditions at the bifurcation node closely follows the two-cell approach originally introduced by Bolla Pittaluga et al. (2003), which accounts for the transverse flux of water (q_y) and sediments (q_{sy}) just upstream the node (see Figure 1). Assuming the downstream branches (*b* and *c*) to have half the width of the upstream channel (*a*), the water and the sediment balance within each node cell, once expressed in dimensionless form, read:

$$q_b=q_a+2\alpha q_y,\quad q_c=q_a-2\alpha q_y, \tag{5}$$

$$2\alpha\frac{d\eta_b^N}{dt}=q_{sa}^O-q_{sb}^I+2\alpha q_{sy},\quad 2\alpha\frac{d\eta_c^N}{dt}=q_{sa}^O-q_{sc}^I-2\alpha q_{sy}, \tag{6}$$

where the cell length has been computed as αW_0^*, where α is an order-1 parameter, and the superscripts *O* and *I* denote the upstream and the downstream end of each cell, respectively, while η^N is the mean bed elevation within each cell (see Figure 1), say for cell *b*,

$$\eta_b^N=\frac{\eta_a^O+\eta_b^I}{2}. \tag{7}$$

According to the BRT model, the sediment exchange between the two cells results from the combined effect of water exchange and gravity due to the transverse bed slope. Thus, the transverse flux of sediment can be given the following dimensionless form:

$$q_{sy}=q_{sa}^O\left[\frac{q_y}{q_a}-\frac{r}{\beta_0\sqrt{\theta_a}}\left(\eta_b^N-\eta_c^N\right)\right], \tag{8}$$

where θ_a is the Shields parameter of the upstream incoming flow and r is an empirical coefficient that measures the gravity effect (Baar et al., 2018).

The model requires the definition of the cell length, that is, of the parameter α, for which different estimates have been adopted in the literature based on empirical calibrations (see tab. 1 of Redolfi, 2023). Physically, the cell length should correspond to the longitudinal spatial scale of two-dimensional effects on flow and bed topography induced by the unequal hydro-morphodynamical response of bifurcates. A first theoretical estimate of α was given by the two-dimensional linear analysis of Redolfi et al. (2016), where it was shown that the critical value of β_0 above which the symmetrical balanced solution becomes unstable, leading to unbalanced equilibrium solutions, coincides with the resonant value β_R that discriminates between prevailing downstream or upstream morphodynamic influence (Zolezzi & Seminara, 2001). Based on this result, and adopting a suitable scaling of the bifurcation cell length that incorporates the dependence of β_R on the Chézy coefficient, Redolfi (2023) provided the following estimate of α:

$$\alpha=\frac{\pi^2}{16}\frac{c^2}{\beta_0}. \tag{9}$$

We note that the triangular step approach adopted herein implies that the bed elevation difference between the node cells in Equation (8) is computed as $(\eta_b^N-\eta_c^N)$, which is half the value $(\eta_b^I-\eta_c^I)$ used in most applications of the BRT model. Therefore, our results are consistent with those of previous works provided we multiply the coefficient α by a factor two.

By substituting (8) into (6), and recalling that the scaling reported in Equation (1) implies that $q_a=1$, we obtain:

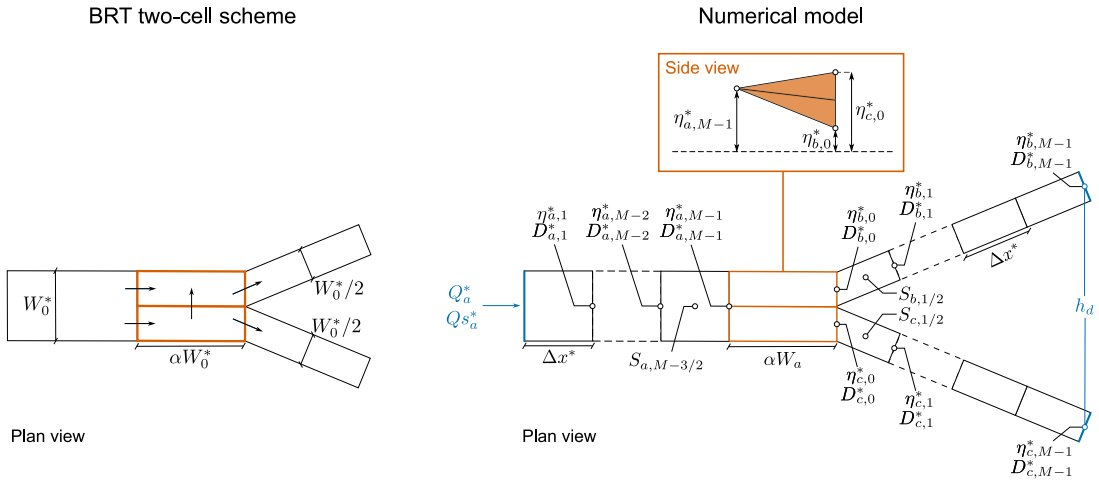

FIGURE 1 Sketch of (a) the two-cell scheme adopted to compute the transverse fluxes of water and sediments and (b) the spatial discretization and boundary conditions of the numerical model. The side view describes the triangular step approach used to model the bed elevation along the node cells.

10969837, 2025, 12, Downloaded from https://onlinelibrary.wiley.com/doi/10.1002/esp.70159 by University Modena, Wiley Online Library on [03/11/2025]. See the Terms and Conditions (https://onlinelibrary.wiley.com/terms-and-conditions) on Wiley Online Library for rules of use; OA articles are governed by the applicable Creative Commons License

$$2\alpha\frac{d\eta_b^N}{dt}=q_{sa}^O\left[q_b-\frac{2\alpha r}{\beta_0\sqrt{\theta_a}}\left(\eta_b^N-\eta_c^N\right)\right]-q_{sb}^I, \tag{10}$$

$$2\alpha\frac{d\eta_c^N}{dt}=q_{sa}^O\left[q_c+\frac{2\alpha r}{\beta_0\sqrt{\theta_a}}\left(\eta_b^N-\eta_c^N\right)\right]-q_{sc}^I. \tag{11}$$

To complete the set of nodal conditions, we impose the water level at the node to be the same in all branches, consistently with all previous applications of the BRT model. This hypothesis, which has proven to be valid for modelling river bars and meandering channels (Camporeale et al., 2007; Struiksma et al., 1985), is likely to hold for any three-dimensional bed disturbance having a length scale of several channel widths (Redolfi, 2021), such as that represented by the node cells. An alternative approach, based on the mechanical energy balance at the node, was proposed by Durante et al. (2024). However, theoretical considerations on two-cell bifurcation models suggest that friction losses are indeed significant (Redolfi, 2023), although their estimate is not trivial, to the point that the authors assumed friction to be negligible in applying the model.

Finally, we note that the values of five dimensionless parameters are required to define the initial configuration in dimensionless form, namely the aspect ratio β_0, the Shields stress θ_0, the length of the bifurcates L, the dimensionless grain size $d_{s0}=D_s/D_0^*$ and the Chézy coefficient c, since the Froude number Fr_0 can be retrieved from the relationship

$$Fr_0^2=c^2\Delta d_{s0}\theta_0, \tag{12}$$

which holds for uniform flow conditions. The results presented in the following sections have been obtained for different combinations of β_0 and L, and fixed values of $\theta_0=0.08$, $d_{s0}=0.01$ and $c=12$.

2.1 | Numerical implementation

We adopt the same numerical model described in Barile et al. (2024), to which we refer to for further details. To integrate Equations (4a), (4b), and (4c) in space and time, we use the finite-difference scheme depicted in Figure 1, in which each of the three branches is discretized by means of M nodes, each identified by means of the index $i=0\ldots M-1$. The morphodynamic evolution of the system is modelled by first computing the flow discharge and water depth along the channels and then updating their bed elevation profiles, according to a decoupled approach. Starting from an initially balanced configuration, we apply a small asymmetric perturbation to the bed elevation of the downstream branches, and we let the bifurcation evolve autonomously over time until a long-term equilibrium condition is achieved. In the following, we briefly describe how the time evolution of the bifurcation is implemented in the numerical model.

The hydrodynamic conditions of the branches are evaluated by means of the gradually varied flow equation, which can be readily derived by combining Equations (4a) and (4b) as

$$\frac{dD}{dx}=\frac{\beta_0}{1-Fr^2}\left(S-\frac{Fr^2}{c^2}\right),\quad Fr^2=Fr_0^2\frac{q^2}{D^3}. \tag{13}$$

At any given time step, the flow discharge in the downstream branches is unknown. Thus, the flow partitioning at the bifurcation node is computed beforehand through an iterative procedure, which relies on the fact that the bed elevation (and therefore the bed slope S) is known at any point of the three branches from the previous time step. Starting from a first guess of the unit discharges q flowing in the bifurcates, Equation (13) is integrated in the upstream direction in both channels by means of a fourth-order Runge–Kutta scheme. The integration starts from the water depth at the downstream end of each branch, which is computed as the difference between the fixed water level and the bed elevation known from the previous time step. As in previous numerical analyses (Barile et al., 2024; Kleinhans et al., 2008), the procedure is then repeated by iterating over q using the Newton–Raphson method, until the water level at the inlet of the branches is the same.

Given the flow discharge flowing in each branch, we retrieve the water-surface profile for each branch for the current iteration. We then compute the Shields stress and the associated transport capacity at each node. Finally, the bed elevation is updated to the following time step by integrating Equation (4c) according to an upwind approach, where the computation of the spatial derivative of the bed elevation takes into account that bed perturbations travel downstream in subcritical conditions.

3 | LINEAR ANALYSIS

A closed-form solution of the governing system of equations derived in Section 2 can be obtained by means of a linear model. The linear analysis takes as reference state the initial equilibrium solution, in which water and sediment are equally distributed in the bifurcates, and flow and sediment transport are uniform in all branches. Previous studies considered a simplified approach, where the evolution of the downstream branches was modelled as a sequence of uniform-flow states (Bolla Pittaluga et al., 2015; Salter et al., 2018). This is justified when analysing the stability of equilibrium solutions because, in their neighbourhood, the evolution is so slow that the downstream channels have enough time to adapt their slope over the entire length, to the point that stability can be analysed also considering a fully-steady approach (Redolfi et al., 2016). However, as will be discussed later, this assumption is not appropriate to determine the timescale of the bifurcation evolution. To overcome this limitation, we need to derive a linear solution that takes into account the spatial and temporal evolution of the downstream branches. To this aim, we first derive the linear solution for a single branch subject to generic, small-amplitude perturbations set at the channel boundaries. We then couple this solution with the nodal point conditions to determine the time evolution of the system. Therefore, differently from canonical linear stability analyses, in this case, the spatial structure is not known a priori and must be retrieved from the coupling between the bifurcation node and the morphodynamic response of the branches.

3.1 | Linear solution for downstream channels

The objective of this section is to determine the solution for a single channel, the boundary conditions of which are slightly perturbed with respect to the reference state (Fasolato et al., 2009). We assume that

10969837, 2025, 12, Downloaded from https://onlinelibrary.wiley.com/doi/10.1002/esp.70159 by University Modena, Wiley Online Library on [03/11/2025]. See the Terms and Conditions (https://onlinelibrary.wiley.com/terms-and-conditions) on Wiley Online Library for rules of use; OA articles are governed by the applicable Creative Commons License

the small-amplitude perturbation of the boundary conditions has a well-defined time structure. Specifically, we consider a perturbation in the harmonic form $e^{\omega t}$, where

$$\omega = \Omega + i\chi \tag{14}$$

is a complex frequency, the real part of which (Ω) is the growth rate of the perturbation, while the imaginary part (χ) is the angular frequency, representing an oscillation in time. This assumption does not limit the generality of the solution, because any variation of the boundary conditions in time can be expanded as a sum of harmonic components, the solutions of which can be determined separately and then recombined thanks to the linear character of the analysis. We note that the timescale of the perturbation must be sufficiently slow to fulfil the quasi-steady hypothesis adopted herein.

Following the standard approach of linear analysis, each variable is expanded in the form:

$$X = X_0 + \delta X_1, \tag{15}$$

where X_0 is the reference state and δ measures the amplitude of perturbation. Substituting into the governing system (4a, 4b, and 4c), expanding in Taylor series around $\delta = 0$ and neglecting higher order terms, we obtain the following linear system:

$$\begin{aligned} &\frac{\partial U_1}{\partial x} + \frac{1}{Fr_0^2}\frac{\partial}{\partial x}(\eta_1 + D_1) + \frac{\beta}{c^2}[2U_1 - D_1] = 0, \\ &\frac{\partial U_1}{\partial x} + \frac{\partial D_1}{\partial x} = 0, \\ &\frac{\partial \eta_1}{\partial t} + 2\Phi_T \frac{\partial U_1}{\partial x} = 0, \end{aligned} \tag{16}$$

where the coefficient

$$\Phi_T = \frac{\theta_0}{\Phi_0}\frac{\partial \Phi}{\partial \theta} \tag{17}$$

measures the sensitivity of the sediment transport rate to variations of the Shields stress. A step-by-step derivation of the linear system (16) is reported in the Supporting Information S1.

The linear system (16) admits solutions of the form:

$$(\eta_1, U_1, D_1) = \left(\tilde{\eta}, \tilde{U}, \tilde{D}\right) e^{\lambda x + \omega t} + c.c., \tag{18}$$

where $c.c.$ denotes the complex conjugate, λ is a complex wavenumber and ω is fixed by the time variation of the boundary conditions. On substituting from (18) into the linear system (16), we obtain the following system of linear algebraic equations:

$$\begin{bmatrix} \frac{\lambda}{Fr_0^2} & \lambda + 2\frac{\beta_0}{c^2} & \frac{\lambda}{Fr_0^2} - \frac{\beta_0}{c^2} \\ 0 & \lambda & \lambda \\ \omega & 2\Phi_T\lambda & 0 \end{bmatrix} \times \begin{bmatrix} \tilde{\eta} \\ \tilde{U} \\ \tilde{D} \end{bmatrix} = \begin{bmatrix} 0 \\ 0 \\ 0 \end{bmatrix}. \tag{19}$$

This system admits three linearly independent, nontrivial solutions, characterized by three different eigenvalues λ_k ($k = 1,2,3$), which can be given the form

$$\left(\tilde{\eta}_k, \tilde{U}_k, \tilde{D}_k\right) = \tilde{D}_k(e_k, u_k, 1) \quad (k = 1,2,3), \tag{20}$$

where the constants $\tilde{D}_k$ are determined by the boundary conditions. The expressions of the eigenvalues λ_k and of the coefficients e_k and u_k are reported in the Supporting Information S1. It is worth noting that one solution is of a degenerate type, being characterized by $\lambda = 0$ and by a vanishing perturbation of the bed elevation. From a physical point of view, this solution reproduces a uniform perturbation of flow velocity and depth caused by a change in the water discharge.

For a given value of the frequency ω, the spatial structure of the solution, say for the bed elevation, is given by a linear combination of three exponential functions, namely:

$$\eta_1 = \left[\tilde{D}_1 e_1 e^{\lambda_1 x} + \tilde{D}_2 e_2 e^{\lambda_2 x} + \tilde{D}_3 e_3 e^{\lambda_3 x}\right] e^{\omega t} + c.c. \tag{21}$$

The three boundary conditions that are required to compute the unknown coefficients $\tilde{D}_k$ depend on the specific problem under investigation. For example, to analyse the effect of sea level rise, we may consider a perturbation of the downstream water level, with fixed (i.e., unperturbed) water and sediment supplies. Conversely, to study the effect of alterations of the sediment availability, we may impose a perturbation of the sediment discharge at the channel inlet, while keeping the downstream water level unperturbed. For the specific case of the downstream branch of a bifurcation, it is of interest to determine the solution driven by a perturbation of the bed elevation set at the channel inlet, having the form

$$\eta_1 = \eta_1^I = \hat{\eta}^I e^{\omega t} + c.c. \quad (x = 0), \tag{22}$$

while assuming the upstream and downstream water levels unperturbed:

$$\eta_1 + D_1 = 0 \quad (x = 0, \quad x = L). \tag{23}$$

Substituting from Equation (21) into the boundary conditions (22) and (23) gives the following linear algebraic system:

$$\begin{aligned} &\tilde{D}_1(e_1 + 1) + \tilde{D}_2(e_2 + 1) + \tilde{D}_3(e_3 + 1) = 0, \\ &\tilde{D}_1(e_1 + 1)e^{\lambda_1 L} + \tilde{D}_2(e_2 + 1)e^{\lambda_2 L} + \tilde{D}_3(e_3 + 1)e^{\lambda_3 L} = 0, \\ &\tilde{D}_1 e_1 + \tilde{D}_2 e_2 + \tilde{D}_3 e_3 = \hat{\eta}^I. \end{aligned} \tag{24}$$

The solution of the above system provides the unknown coefficients $\tilde{D}_k$ as functions of the upstream boundary parameters $\hat{\eta}^I$ and ω (Equation 22) and of the channel length L. It is worth noting that at this stage the frequency ω is still undetermined, since its actual value is controlled by the coupling with the bifurcation, as detailed in Section 3.2. We also note that in the limit case of a vanishing perturbation of the inlet bed elevation the trivial (unperturbed) solution is retrieved.

Once the coefficients are calculated, it is possible to compute the perturbations of the unit water discharge (q_1) and of the sediment transport capacity (q_{s1}) at the channel inlet, which are fundamental ingredients in the analysis of the evolutionary timescale of bifurcations presented in the next section. By adopting a structure similar to Equation (22), we can write those quantities as

10969837, 2025, 12, Downloaded from https://onlinelibrary.wiley.com/doi/10.1002/esp.70159 by University Modena, Wiley Online Library on [03/11/2025]. See the Terms and Conditions (https://onlinelibrary.wiley.com/terms-and-conditions) on Wiley Online Library for rules of use; OA articles are governed by the applicable Creative Commons License

$$q_1^I = q_\eta(\omega)\,\eta_1^I, \quad q_{s1}^I = q_{s\eta}(\omega)\,\eta_1^I. \tag{25}$$

The expressions of the coefficients q_η and $q_{s\eta}$ are reported in the Supporting Information S1.

3.2 | Coupled solution for the bifurcation-downstream channels system

To derive the coupled solution for the bifurcation-downstream channels system, we first linearize the nodal point conditions. Recalling the decomposition (15), from the water balance (5) we obtain:

$$q_{b1} = -q_{c1}. \tag{26}$$

Similarly, from the mass balance equations (10) and (11), by considering the linear terms only, we derive the following relations:

$$2\alpha\frac{d\eta_{b1}^N}{dt} = q_{b1} + q_{sa1}^O - q_{sb1}^I - \frac{2\alpha r}{\beta_0\sqrt{\theta_0}}\left(\eta_{b1}^N - \eta_{c1}^N\right), \tag{27}$$

$$2\alpha\frac{d\eta_{c1}^N}{dt} = q_{c1} + q_{sa1}^O - q_{sc1}^I + \frac{2\alpha r}{\beta_0\sqrt{\theta_0}}\left(\eta_{b1}^N - \eta_{c1}^N\right). \tag{28}$$

The full linearization procedure of the nodal point conditions is reported in the Supporting Information S1.

Finally, the condition of equal water level H at the entrance of the bifurcates gives

$$H_{b1}^I = H_{c1}^I. \tag{29}$$

From a linear perspective, the coupling between the single-channel solution and the nodal point relations is facilitated by symmetry considerations. Specifically, the instability process can be studied by considering a perfectly antisymmetric solution, in which the perturbation in channel c is equal and opposite to that in channel b (i.e., $\eta_{b1} = -\eta_{c1}$, $D_{b1} = -D_{c1}$, $q_{b1} = -q_{c1}$, $q_{sb1} = -q_{sc1}$) and the solution in channel a is unperturbed ($\eta_{a1} = 0$, $D_{a1} = 0$, $q_{a1} = 0$, $q_{sa1} = 0$). It is immediate to verify that this solution satisfies (26) and (29). Moreover, it implies that once the sediment continuity equation (27) for cell b is satisfied, the corresponding continuity equation (28) for cell c is also ensured. Finally, if the solution for channel b satisfies the system, the same is also valid for the opposite solution for channel c. These considerations allow us to derive the coupled solution by considering only half of the system (i.e., cell b and channel b).

Given the above specifications, and setting $\eta_{b1}^N = \eta_{b1}^I/2$ according to Equation (7), we can express Equation (27) in terms of quantities evaluated at the inlet of channel b as

$$\alpha\frac{d\eta_{b1}^I}{dt} = q_{b1}^I - q_{sb1}^I - 2\frac{r\alpha}{\beta_0\sqrt{\theta_0}}\eta_{b1}^I, \tag{30}$$

while an identical relation is obtained from Equation (28) for channel c.

If we consider a perturbation of the bed elevation at the channel inlet of the form (22), the associated response of the sediment and water discharges at the inlet can be computed using Equation (25). On substituting into Equation (30) and simplifying η_{b1}^I, we obtain the following dispersion relation:

$$\alpha\omega + 2\frac{r\alpha}{\beta_0\sqrt{\theta_0}} - q_\eta(\omega) + q_{s\eta}(\omega) = 0, \tag{31}$$

which can be numerically solved to determine the complex frequency ω as a function of the parameters of the reference state and of the length of the bifurcates.

The stability of the initial reference configuration depends on the sign of the real part of ω, that is, on the growth rate Ω. A negative value of Ω implies that the linear perturbation decays over time and the reference state is stable, while a positive value means that the bifurcation evolves towards an unbalanced configuration, characterized by an uneven distribution of the water and sediment discharges in the bifurcates. It is worth noting that for all the unstable cases (i.e., when $\beta_0 > \beta_R$), the imaginary parts of the three eigenvalues λ_k ($k = 1,2,3$) and of the complex frequency ω are found to vanish, which implies that the solutions of the problem do not oscillate in space or time. From the linear analysis we then derive the following estimate of the evolutionary timescale of bifurcations:

$$T_{BIF} = \frac{1}{\Omega}. \tag{32}$$

4 | RESULTS

4.1 | Transient behaviour of bifurcations

Consistent with the results of previous analyses, both the linear model and the numerical simulations predict that any perturbation of the reference balanced configuration is amplified over time, that is, its growth rate Ω is positive, when the aspect ratio β_0 exceeds the critical threshold β_R. The latter parameter depends on the values of Shields stress and Chézy coefficient of the reference configuration (as shown in fig. 6 of Redolfi et al., 2019).

In the following, we first outline the morphodynamic evolution of super-critical bifurcations towards their long-term unbalanced configuration, as it results from the outcomes of the numerical simulations. We use the subscripts b and c to denote the "dominant" and "nondominant" branch, respectively, and we define the discharge asymmetry ΔQ as

$$\Delta Q := \frac{W_b^* q_b^* - W_c^* q_c^*}{W_0^* q_0^*} = \frac{1}{2}(q_b - q_c). \tag{33}$$

As the bed elevation gap between the two cells (i.e., the "inlet step") develops, the water and sediment discharges carried by the dominant branch increase over time, while they both decrease for the other branch. These variations cause an unbalance between the sediment supply and the transport capacity in both branches, leading to aggradation in the nondominant branch and erosion in the dominant branch.

The morphological evolution of a bifurcation with relatively short branches ($L = 2 \cdot 10^2$) is described in the upper panels of Figure 2, which show the bed elevation profiles—plotted at different time steps

10969837, 2025, 12, Downloaded from https://onlinelibrary.wiley.com/doi/10.1002/esp.70159 by University Modena, Wiley Online Library on [03/11/2025]. See the Terms and Conditions (https://onlinelibrary.wiley.com/terms-and-conditions) on Wiley Online Library for rules of use; OA articles are governed by the applicable Creative Commons License

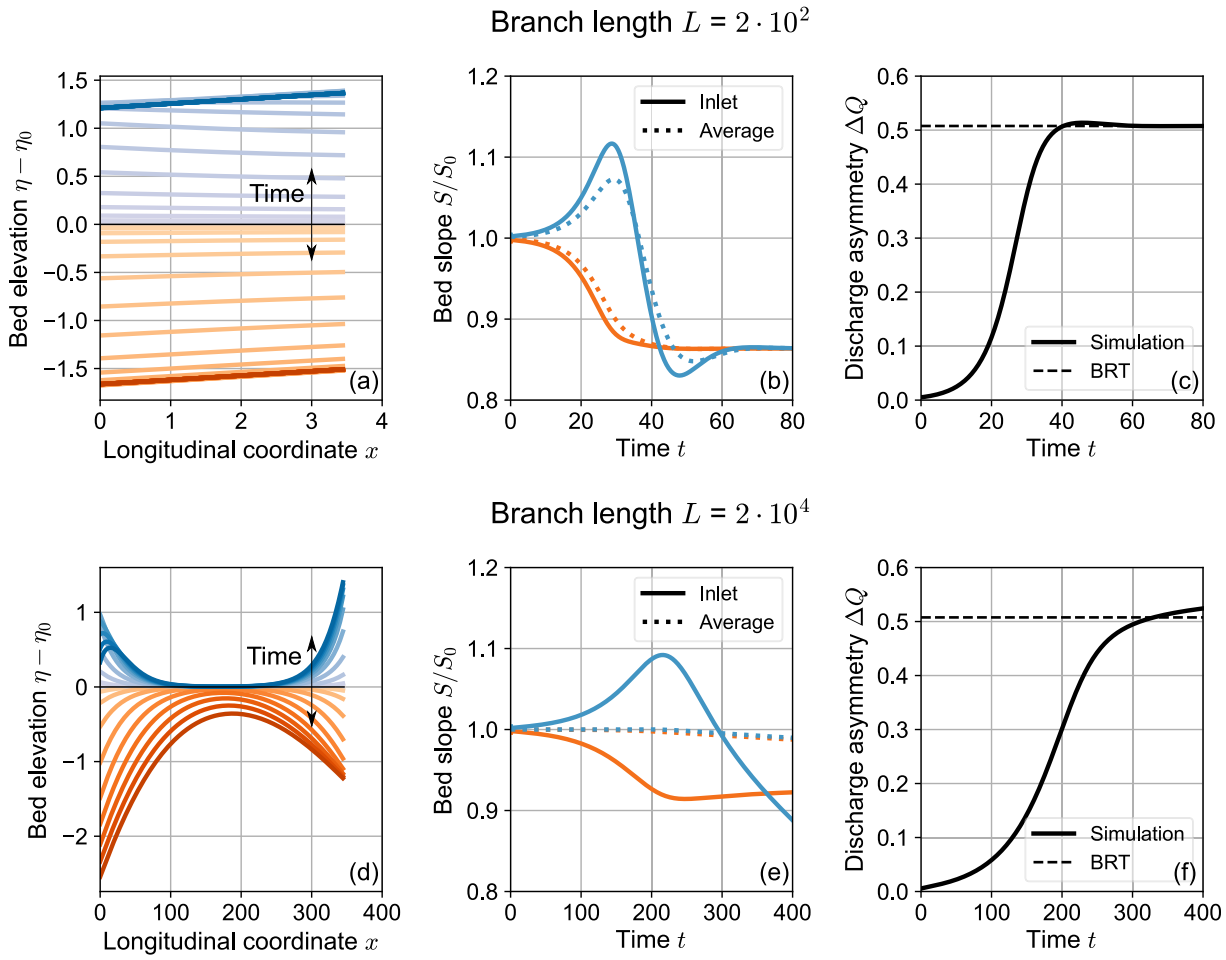

FIGURE 2 Spatio-temporal morphological evolution of the bifurcates in two simulations having the same reference flow and geometry, except for the length of the branches L. The two colours in panels (a,b,d,e) refer to the two bifurcates, namely the aggrading, "nondominant" branch and the eroding, "dominant" branch. The upper panels illustrate a simulation with short branches ($L = 2 \cdot 10^2$), while the lower panels are referred to a simulation with long branches ($L = 2 \cdot 10^4$). (a,d) The scaled bed elevation profiles of the bifurcates retrieved for different time steps throughout the simulation, obtained by subtracting the initial bed profile η_0. (b,e) The inlet (solid lines) and average (dotted lines) bed slope of the branches, scaled with the reference slope S_0. (c,f) The discharge asymmetry ΔQ (defined in Equation 33) between the bifurcates (solid line) and the long-term equilibrium value computed by means of the BRT analytical model (dashed line). We note that the final bed elevation profiles of the long branches simulation (d) refer to the dimensionless time $t = 400$, at which the bifurcates have not yet achieved equilibrium, although the flow discharge asymmetry already reached its equilibrium value. The scaled aspect ratio of both simulations is equal to $(\beta_0 - \beta_R)/\beta_R = 0.45$.

of the simulation—along with the bed slope of the bifurcates and the discharge asymmetry. From the very beginning of the simulation, as the initial small perturbation starts being amplified, the bed slopes at the inlets of the bifurcates take two diverging trajectories, as shown in Figure 2b. Specifically, the inlet bed slope of the aggrading, nondominant branch increases due to local deposition, while the bed slope at the inlet of the dominant branch decreases due to erosion. The resulting exponential growth (decay) of the bed slope at the inlet of the nondominant (dominant) branch in the initial stage resembles the typical behaviour of unstable linear dynamical systems. This evidence suggests that the assumption of equal and constant bed slopes, as employed in previous studies, is not fulfilled even for small perturbations of the balanced configuration.

The initial response of the inlet bed slopes provides a negative feedback to the water and sediment partition at the node, since a larger bed slope at the inlet of the nondominant branch increases its ability to capture water and sediments from the node (and vice versa for the dominant branch). As will be shown later, this effect slows down the evolution of the bifurcation, making the resulting timescale much longer than that obtained by assuming the constancy over time of the bed slope of the branches.

As the bifurcation further develops, the inlet bed slope of the nondominant branch reaches a maximum point and then starts decreasing, while the dominant branch keeps eroding, further decreasing its inlet bed slope. Meanwhile, the asymmetry in the water and sediment discharges and the inlet step keep increasing monotonically, and attain values that are close to those corresponding to the long-term equilibrium solution predicted by the BRT model (Figure 2c). It is worth noting that this happens before the bifurcates have reached their overall morphodynamic equilibrium, that is, a constant bed slope and uniform flow conditions.

In the following stage, the partitioning of water and sediment between the bifurcates does not change significantly throughout the simulation, let aside a small "overshoot" with respect to the final equilibrium value. Meanwhile, both branches keep adapting their bed slope to the water and sediment supply delivered by the bifurcation node, progressively evolving towards their long-term equilibrium bed slope, which matches that predicted by the BRT model.

10969837, 2025, 12, Downloaded from https://onlinelibrary.wiley.com/doi/10.1002/esp.70159 by University Modena, Wiley Online Library on [03/11/2025]. See the Terms and Conditions (https://onlinelibrary.wiley.com/terms-and-conditions) on Wiley Online Library for rules of use; OA articles are governed by the applicable Creative Commons License

By looking at the evolutionary trajectory of a bifurcation with much longer branches $\left(L = 2 \cdot 10^4\right)$, reported in the lower panels of Figure 2, one can readily see that the evolution of the inlet bed slopes during the first phase of numerical simulations does not change qualitatively with respect to the simulation with shorter branches. Moreover, as in the case of short branches, the discharge asymmetry ΔQ reaches approximately its long-term equilibrium value when the inlet bed slope of the nondominant branch peaks, therefore well before the overall equilibrium configuration of the bifurcation is established.

Contrary to the evolution of the inlet bed slopes of the bifurcates, the trend of the average bed slopes does show a significant dependence on the length of the branches, due to the spatial variability of the morphological evolution of the bifurcates. For relatively short branches, the aggradation and degradation processes occur homogeneously along the whole length of both branches. Although the variation of the bed slope is larger near the inlet of the branches, as shown by Figure 2b, the resulting bed elevation profiles remain almost linear throughout the simulation (Figure 2a), leading the inlet and the average bed slope to follow qualitatively similar trends over time. On the contrary, in the case of long branches the aggradation and degradation processes are not uniformly distributed along the branches. In fact, the morphological processes induced in the bifurcates by changes in the water and sediment supply are concentrated near the upstream and downstream end of the branch, leaving the middle reach of the nondominant branch unperturbed (Figure 2d). At the upstream end of the branch, a downstream-prograding front generates a sequence of concave-up bed profiles. At the same time, the bed elevation at the branch inlet increases over time as the corresponding node cell keeps aggrading. We note that the morphodynamic behaviour displayed by the nondominant, aggrading branch follows that of real bifurcations, where prograding fronts characterize the evolution of the minor branch (Szewczyk et al., 2020; Szewczyk et al., 2022). After reaching its peak value, the inlet bed slope of the branch starts decreasing (as in the simulations with shorter branches, Figure 2b,e), while the depositional wave further migrates downstream. At the opposite side of the channel, the bed elevation profile is influenced by the downstream boundary condition of constant water level. This condition implies that, as the water discharge decreases, the transport capacity decreases over time near the channel outlet, generating an upstream-migrating prograding front that reduces the local bed slope. While the two aggradational waves propagate in the nondominant branch, two analogous albeit erosional waves generate at both ends of the dominant branch (Figure 2d), leading its bed elevation profile to become convex upward. Due to the combined, counteracting effect on the local bed slope of these aggradational and erosional waves, the average bed slopes of both bifurcates remain almost constant during the first evolutionary phase of the bifurcation (Figure 2e).

The bed elevation profiles observed in the bifurcation with long branches suggest that the morphodynamic evolution of the bifurcates is driven by two distinct unsteady processes, namely the changes in the water and sediment supply determined by the evolution of the bifurcation node and the feedback triggered by the downstream boundary condition. Contrary to the bifurcation with long branches (Figure 2d), the bifurcation with short branches shows homogeneous erosion and deposition along its bifurcates (Figure 2a), suggesting that the two processes start interacting from the very beginning of its morphodynamic evolution. As discussed in the following, this evidence suggests that the downstream boundary condition and the length of the bifurcates play a relevant role in determining the timescale of bifurcations with short branches.

We note that simulations in which the sediment transport ceases in one branch, as it occurs at large values of the reference aspect ratio β_0, display in the first evolutionary stage a behaviour that resembles that described so far for bifurcations where both branches actively transport sediments. However, the long-term equilibrium does not match that predicted by the BRT model and may change considerably with the branch length, ranging from the partial to the complete closure of one branch (Barile et al., 2024).

4.2 | The bifurcation timescale

Based on the results of the numerical simulations reported in Figure 2, the transient behaviour of a bifurcation evolving from an initial balanced unstable configuration to an unbalanced equilibrium configuration can be divided into two phases, each of which is characterized by a specific timescale. Regardless of the length of the bifurcates, the time required by the distribution of the water and sediment fluxes delivered by the node to reach a value close to the final equilibrium is much shorter than that needed to achieve the overall morphodynamic equilibrium of the downstream branches.

If we consider the first phase of the process, an estimate of the inherent timescale (T_{BIF}) of adaptation to equilibrium of water and sediment partitioning at the node can be obtained both on the basis of the linear analysis (Equation 32), and by analysing the initial growth rate of the discharge asymmetry retrieved from the numerical simulations. To do so, we compute the timescale T_{BIF} as the value that ensures the best fit between the exponential function

$$\Delta Q(t) = \Delta Q(0)\, e^{t/T_{BIF}} \tag{34}$$

and the numerical results (Figure 3).

The resulting values of T_{BIF} are reported in Figure 4 as a function of the branch length L, for different values of the scaled aspect ratio $\epsilon = (\beta_0 - \beta_R)/\beta_R$, which provides a measure of the distance of the reference aspect ratio β_0 from the critical value for the stability of balanced bifurcations. The results of both the numerical simulations and the analytical model, which exhibit a very good agreement, show that T_{BIF} decreases as the parameter ϵ gets larger. In the parameter space explored in the Figure ($\epsilon \in [0.15, 0.6]$, $L \in \left[10^2, 10^5\right]$), T_{BIF} ranges from 10^0 to 10^2, that is, 1 to 100 times the Exner timescale (defined as in Equation 2).

The bifurcation timescale T_{BIF} markedly depends on the branch length, as highlighted in Figure 4. For low values of L, and regardless of the value of ϵ, T_{BIF} exhibits a nonlinear increase with the branch length. We note that in this case the downstream boundary condition affects the morphodynamic evolution of the bifurcates up to their inlet, as shown by panels a and b of Figure 2. For longer branches, the curves $T_{BIF}(L)$ reach a plateau for any value of the scaled aspect ratio, revealing that T_{BIF} becomes independent of the branch length. This asymptotic value of T_{BIF} represents the evolutionary timescale of bifurcations with "long branches" (depicted in the lower panels of Figure 2), in which the downstream condition does not affect the

10969837, 2025, 12, Downloaded from https://onlinelibrary.wiley.com/doi/10.1002/esp.70159 by University Modena, Wiley Online Library on [03/11/2025]. See the Terms and Conditions (https://onlinelibrary.wiley.com/terms-and-conditions) on Wiley Online Library for rules of use; OA articles are governed by the applicable Creative Commons License

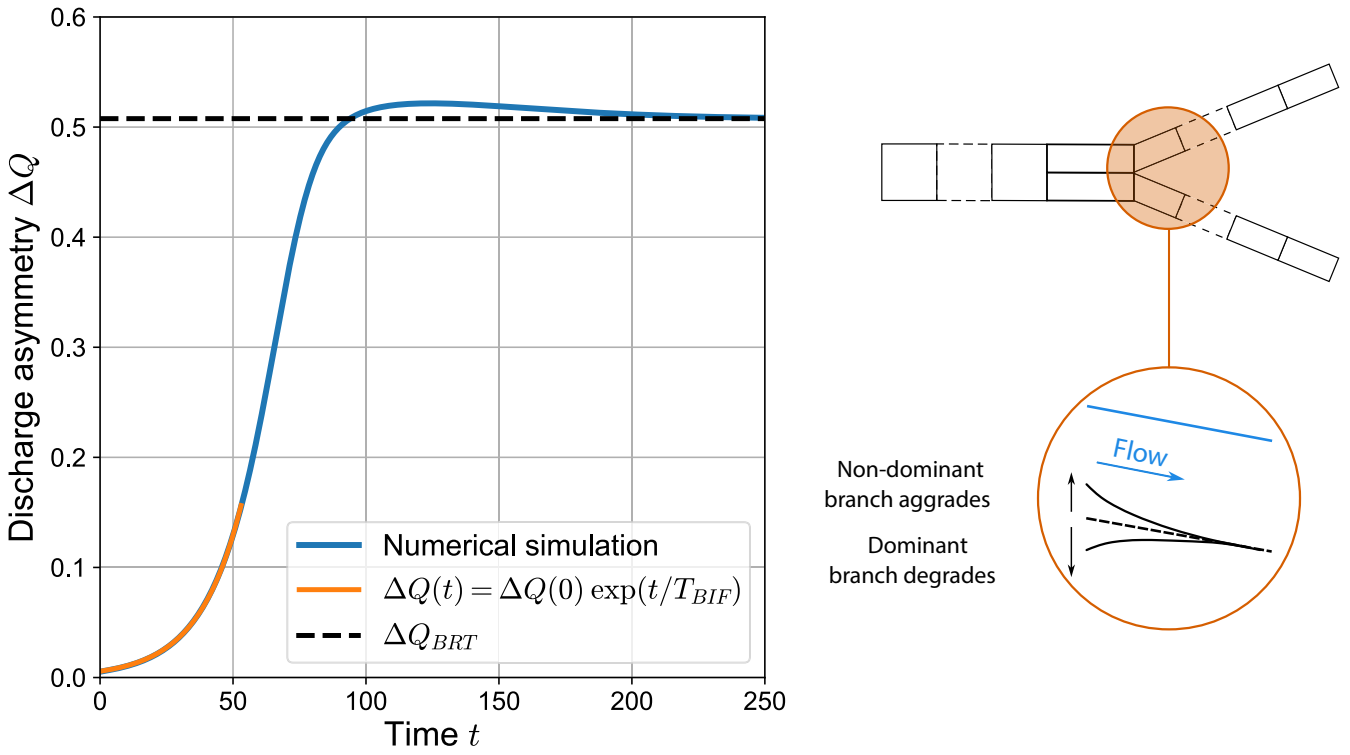

FIGURE 3 Computation of the bifurcation timescale T_{BIF} from the results of numerical simulations: T_{BIF} is computed as the value that makes the exponential function described in Equation (34) the best fit for the first stage of the $\Delta Q(t)$ curve returned by the numerical simulation. The sketch in the circle describes the physical process the timescale refers to. The simulation parameters used are $L = 1000$, $(\beta_0 - \beta_R)/\beta_R = 0.45$.

first evolutionary stage at the inlet of the bifurcates. The above results reveal that the influence of the downstream condition speeds up the adaptation to equilibrium of the water and sediment distribution at the node.

Concerning the dependence of the bifurcation timescale T_{BIF} on the scaled aspect ratio ϵ, Figure 4b reveals that by multiplying T_{BIF} by ϵ the residual dependence on ϵ becomes negligible for small values of L, which implies that in the limit of short branches the dependence of T_{BIF} on the scaled aspect ratio is well described by the relation

$$T_{BIF} \sim 1/\epsilon. \tag{35}$$

We note that Equation (35) implies that as $\epsilon \to 0$ (i.e., as $\beta_0 \to \beta_R$) T_{BIF} goes to infinity, that is, the growth rate vanishes.

For long branches, T_{BIF} exhibits a different dependence on ϵ, as shown by the logarithmic plot of Figure 5, where the relationship between T_{BIF} and ϵ obtained via the linear model is reported for different lengths L of the bifurcates. The curve corresponding to the asymptotic limit of "long branches" ($L \to \infty$) has a slope value of -2 when ϵ is small, which indicates an inverse quadratic dependence of T_{BIF} on ϵ. Furthermore, its slope in the log–log plot decreases as ϵ increases, reaching a value between -2 and -1. For low values of L, the curves $T_{BIF}(\epsilon)$ behave according to Equation (35) regardless of the value of ϵ. The same behaviour is displayed by the curves corresponding to bifurcations with long branches only at small values of ϵ, while they approach the asymptotic limit of "long branches" as ϵ gets larger.

As outlined in the previous section, simulation results provide clear evidence of the presence of two distinct stages in the transient behaviour of bifurcations. Specifically, the two stages can be identified by analysing the results of numerical simulations in terms of the time variable rescaled by T_{BIF}, as done in Figure 6 for the discharge asymmetry ΔQ and for the scaled bed slope S/S_0 at the inlet of the bifurcates. Considering simulations with different values of L (spanning three different orders of magnitude), these curves tend to collapse in the first evolutionary stage, which lasts approximately 5 T_{BIF}. Within this time span, both the inlet step and the discharge asymmetry attain their long-term equilibrium values. On the contrary, the evolutionary trajectories display a marked residual dependence on L in the second stage, during which the downstream branches adapt their slopes to the long-term equilibrium value, while the incoming water and sediment discharges remain nearly constant. Specifically, as described by Figure 6b, the longer the branches, the larger the difference between the bed slope resulting from the first phase and that reached in the long term. Therefore, the adaptation process is longer for bifurcations with longer branches.

4.3 | Insights on the morphological response of the bifurcates

The linear model derived in Section 3 allows for an in-depth analysis of the transient behaviour of an evolving bifurcation by investigating the role of the two main processes that influence the morphological evolution of the bifurcates, namely, the changes in the distribution of water and sediment discharges delivered by the upstream node and the feedback exerted by the downstream boundary condition. To do so, we find it convenient to explore the response of any of the two downstream branches by separating the effects of the perturbations of the water and sediment supply. Furthermore, we assume that the

10969837, 2025, 12, Downloaded from https://onlinelibrary.wiley.com/doi/10.1002/esp.70159 by University Modena, Wiley Online Library on [03/11/2025]. See the Terms and Conditions (https://onlinelibrary.wiley.com/terms-and-conditions) on Wiley Online Library for rules of use; OA articles are governed by the applicable Creative Commons License

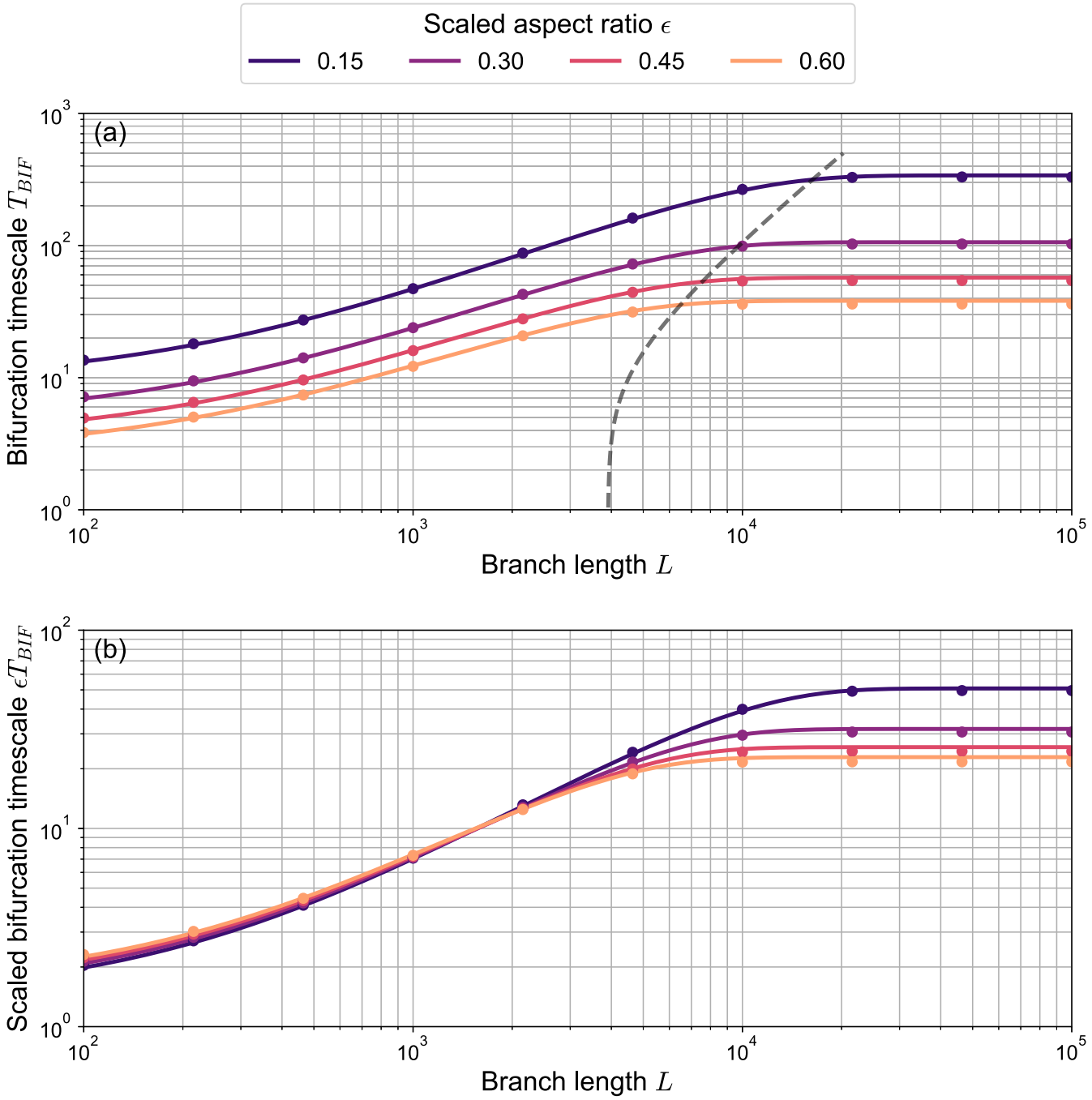

FIGURE 4 Bifurcation timescale T_{BIF} as a function of the dimensionless length of the branches L, for different values of the distance from critical conditions $\epsilon = (\beta_0 - \beta_R)/\beta_R$. Solid lines show the results of the linear model, while dots indicate the values returned by the numerical simulations. The dashed line indicates the "long branches" threshold L_{LB}, as derived by means of the linear model (Equation 37). When the timescale T_{BIF} is multiplied by the parameter ϵ, as in panel (b), the curves collapse on a single curve for small values of L.

channel is long enough to prevent the downstream boundary condition from affecting the evolution of the bifurcation node, thus considering the case of a bifurcation with "long" branches.

In general, the linear model allows for setting an arbitrary perturbation of the upstream boundary condition by choosing a value of the complex frequency ω (see Equation 14). However, the solution of the dispersion relation (31) suggests that in the case of an evolving bifurcation node with $\beta_0 > \beta_R$ the three eigenvalues λ_k ($k = 1,2,3$) and the complex frequency ω are real numbers. We then take $\chi = 0$ and assume an arbitrary and positive value of the growth rate Ω, or equivalently of the timescale $T = 1/\Omega$. We note that in the case of a bifurcation the actual value of the perturbation timescale T corresponds to T_{BIF} and results from coupling the response of the downstream channels with that of the bifurcation node (see Section 3). Figure 7 describes how the three eigenvalues λ_k depend on the growth rate Ω. It is worth noting that λ_2 and λ_3 show similar values but opposite sign, which indicates that the length of influence of the upstream and downstream boundary conditions is comparable. The nearly parabolic shape of the curves suggests that the spatial scale roughly depends on the square root of the timescale, which is a characteristic feature of diffusive processes.

Let us first consider the case of a decrease in the incoming water discharge (for a fixed sediment supply), that is, of a negative value of the perturbation of the unit discharge q_1^l. The resulting distributions

10969837, 2025, 12, Downloaded from https://onlinelibrary.wiley.com/doi/10.1002/esp.70159 by University Modena, Wiley Online Library on [03/11/2025]. See the Terms and Conditions (https://onlinelibrary.wiley.com/terms-and-conditions) on Wiley Online Library for rules of use; OA articles are governed by the applicable Creative Commons License

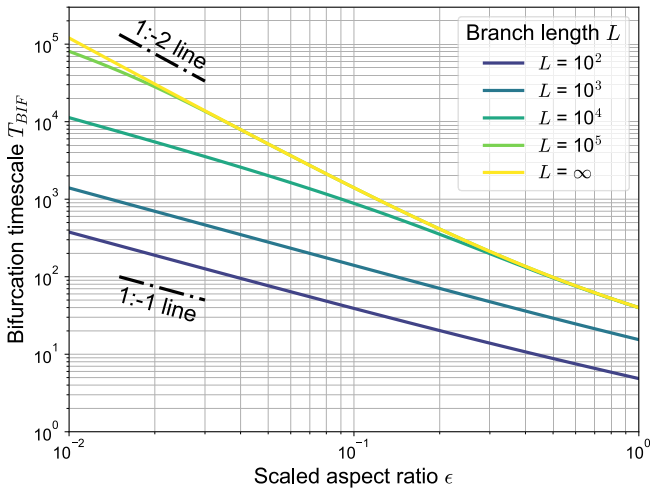

FIGURE 5 Dependence of the dimensionless bifurcation timescale T_{BIF} on the scaled aspect ratio $\epsilon = (\beta_0 - \beta_R)/\beta_R$, computed using the linear model for different values of the dimensionless length of the branches L.

along the channel of the perturbations of flow and bed elevation are reported in Figure 8a. We note that the linear solution captures the same features displayed by the results of numerical simulations with long branches (see Figure 2d). Specifically, the response of the channel is composed of three distinct phenomena.

1. In the central part of the channel the bed is nearly unperturbed, and the flow remains uniform. However, both the water depth and the flow velocity perturbations are negative, to accommodate the decrease in the water discharge. This effect is associated with the null eigenvalue λ_1, which produces a spatially invariant perturbation.
2. In the downstream part of the channel the bed aggrades to accommodate the downstream boundary condition, which prescribes an unperturbed water surface elevation. Due to the decrease in the water discharge, the downstream water level produces a M1-type backwater profile, which leads to flow deceleration and sediment deposition. Recalling the structure of the linear solution (Equation 18), this effect manifests itself as an exponentially decaying perturbation in the upstream direction associated with the positive eigenvalue λ_2.
3. In the upstream part of the channel, the bed aggradation is due to the decrease in the sediment transport capacity, which outpaces that of the sediment supply. The extent of the upstream deposition corresponds to the so-called "boundary layer", as described by Wong and Parker (2006). This effect is associated with the negative eigenvalue λ_3, which produces an exponentially damped solution in the downstream direction.

Unlike the previous case, the effect of a decrease in sediment supply (given a fixed water discharge), that is, of a negative value of the perturbation of the unit sediment discharge q_{s1}^I, remains confined within the upstream part of the channel, as shown in Figure 8b. In this case the only nonvanishing linear solution is that associated with the negative eigenvalue λ_3, which produces local bed degradation and a consequent slight decrease in the water velocity. It is worth highlighting that analogous results are obtained by increasing the water and sediment supply, except for the fact that the sign of all perturbations is reversed. Therefore, for a given value of the timescale T the linear solution for the two bifurcates is identical, except for the sign of perturbations.

The results described above allow us to compute the minimum branch length L_{LB} for which the bifurcation node evolves independently of the downstream boundary condition, that is, for which the bifurcation displays the "long branches" behaviour. To do so, we define the parameters

$$\Lambda_k = \frac{2}{|\lambda_k|}, \quad k = 2, 3, \tag{36}$$

which measure the length of influence of the boundary conditions, that is, the distance from the downstream (Λ_2) and the upstream (Λ_3) end of the bifurcates, respectively, at which the amplitude of the perturbations produced by the boundary conditions decay by a factor $e^{-2} \simeq 0.135$ (see Figure 8). For a given value of the perturbation timescale T, the threshold length L_{LB} can thus be estimated as

$$L_{LB} = \Lambda_2 + \Lambda_3. \tag{37}$$

As reported in Figure 4a, the "long branches" threshold L_{LB} computed using Equation (37) accurately identifies, for the different values of the scaled aspect ratio ϵ, the value above which the bifurcation timescale no longer depends on the length of the branches L. We note that the lengths of influence Λ_2 and Λ_3 increase as the growth rate of the perturbations decreases, as shown in Figure 7. Therefore, the smaller the parameter ϵ, the larger the value of L_{LB}. In other words, when the aspect ratio β_0 is closer to the critical value β_R, that is, for slowly evolving bifurcations, a greater branch length is required to meet the "long branches" asymptotic behaviour.

The response of the downstream branches of an evolving bifurcation is a combination of those displayed in the two panels of Figure 8, since both the water and sediment supply change in each bifurcate over time as a result of the evolution of the inlet bed elevation. If we consider the nondominant aggrading branch, a positive perturbation of the bed elevation (η_1) set at the inlet implies a negative perturbation of the unit water (q_1) and sediment (q_{s1}) discharges, as described in Figure 9a. We note that q_1 is constant along the branch, while the reduction in transport capacity, that is, the absolute value of q_{s1}, locally increases along the upstream and downstream parts of the branch, where bed aggradation occurs. The bed slope perturbation S_1 varies accordingly to the bed profile perturbation, shifting from positive values in the steeper upstream reach to negative values in the milder downstream reach and vanishing in the middle reach, where also the bed elevation is unperturbed.

Overall, the perturbation of the transport capacity is notably larger than that of the flow discharge, as also shown in Figure 9b, where the values of q_1 and q_{s1} computed at the inlet of the nondominant branch are reported for different values of the scaled aspect ratio ϵ. We note that such an overreaction of the transport capacity to changes in the inlet bed elevation is necessary to ensure a positive value of the growth rate, that is, the evolution of the bifurcation towards an unbalanced state. In fact, when $\epsilon > 0$ Equation (31) reduces to

10969837, 2025, 12, Downloaded from https://onlinelibrary.wiley.com/doi/10.1002/esp.70159 by University Modena, Wiley Online Library on [03/11/2025]. See the Terms and Conditions (https://onlinelibrary.wiley.com/terms-and-conditions) on Wiley Online Library for rules of use; OA articles are governed by the applicable Creative Commons License

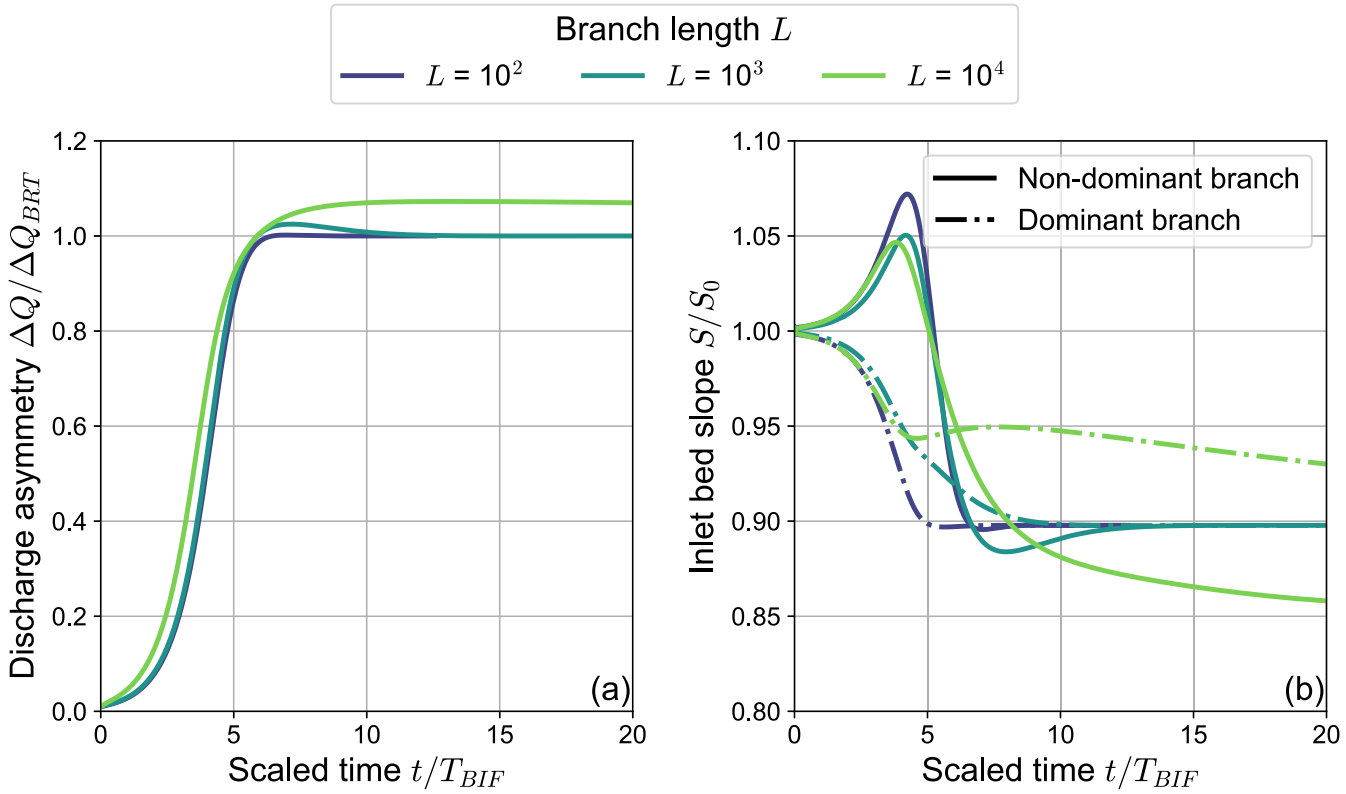

FIGURE 6 Time evolution of (a) the water discharge asymmetry and (b) the bed slope at the inlet of the bifurcates, retrieved from three different numerical simulations, spanning three orders of magnitude for the branch length *L*. The time variable *t* is normalized with the timescale T_{BIF}. The scaled aspect ratio of all simulations is equal to $\epsilon = (\beta_0 - \beta_R)/\beta_R = 0.3$.

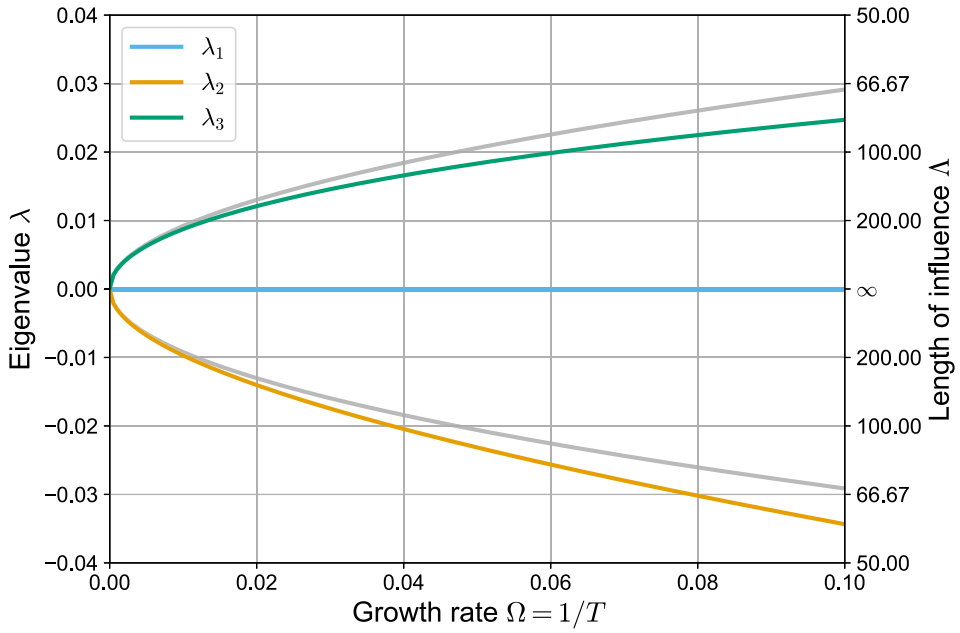

FIGURE 7 The three spatial eigenvalues λ_k $(k = 1,2,3)$ and the corresponding lengths of influence Λ_k (computed according to Equation 36) as functions of the growth rate $\Omega = 1/T$ of the imposed perturbation (Equation 22), considering a vanishing angular frequency χ. When $\chi = 0$ and $\Omega > 0$, all eigenvalues are found to be real (i.e., no spatial oscillations). The gray lines represent the values calculated by means of the diffusive solution.

$$\alpha\Omega = q_\eta - q_{s\eta} - \frac{2r\alpha}{\beta_0\sqrt{\theta_0}}. \tag{38}$$

According to Equation (25), both q_η and $q_{s\eta}$ are negative functions, because a positive (negative) perturbation of the bed level at the inlet implies a reduction (increase) of the water and sediment discharges in the nondominant (dominant) branch. As the last term on the right-hand side of Equation (38) is invariably negative, this implies that $\Omega > 0$ requires $|q_{s1}| > |q_1|$.

Increasing the value of ϵ, the flow and sediment transport perturbations at the inlet decrease (as well as the difference between the two), while the bed slope gets larger (Figure 9c), that is,

10969837, 2025, 12, Downloaded from https://onlinelibrary.wiley.com/doi/10.1002/esp.70159 by University Modena, Wiley Online Library on [03/11/2025]. See the Terms and Conditions (https://onlinelibrary.wiley.com/terms-and-conditions) on Wiley Online Library for rules of use; OA articles are governed by the applicable Creative Commons License

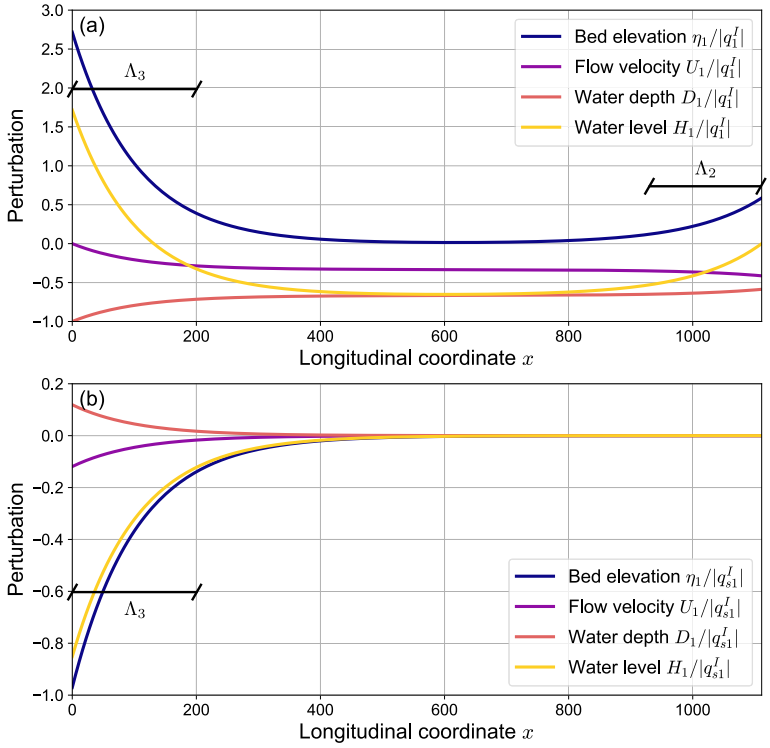

FIGURE 8 Spatial structure of the linear solution for a "long" channel ($L = 2 \cdot 10^4$) subject to a reduction of (a) the upstream water discharge and (b) the sediment supply. The different lines describe the trends along the bifurcate of the perturbations of the bed elevation η_1, flow velocity U_1, water depth D_1 and free-surface elevation H_1, scaled by the absolute values of the imposed (a) unit discharge q_1^I and (b) unit sediment supply q_{s1}^I perturbations at the channel inlet. Example with perturbation timescale $T = 10^2$.

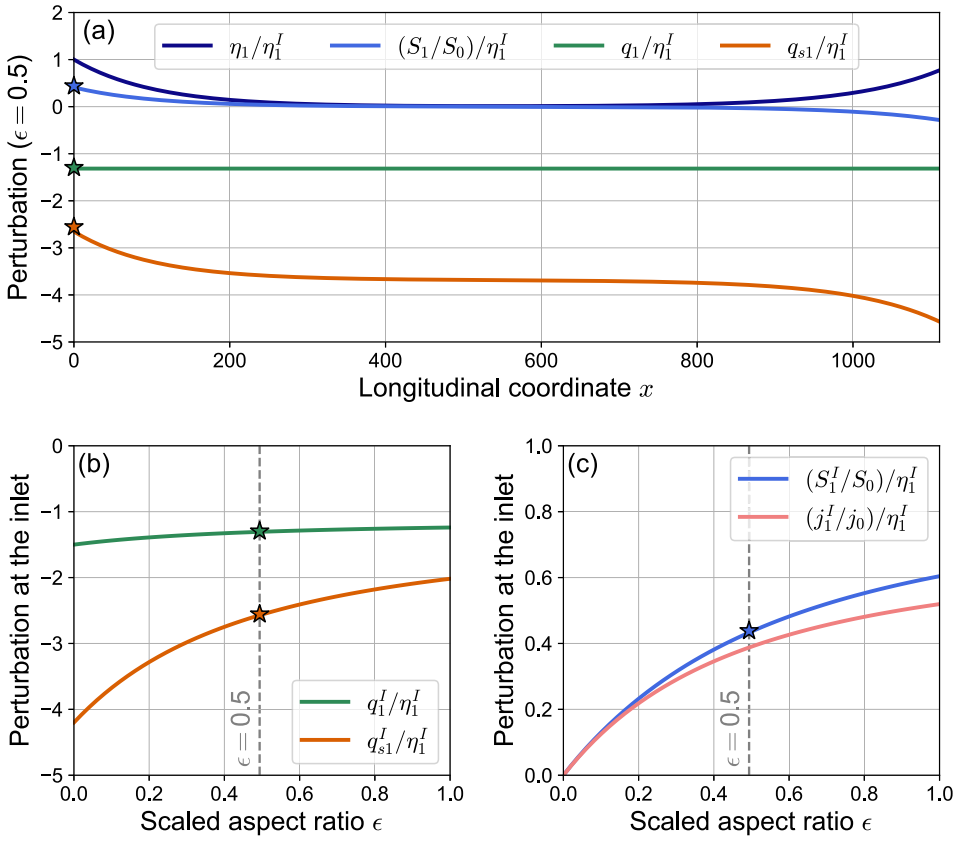

FIGURE 9 The response of the nondominant branch of an evolving bifurcation, as returned by the linear model. The upper panel (a) shows the trends along the bifurcate of the perturbations of the bed slope S_1, the unit discharge q_1 and the unit transport capacity q_{s1}, associated with a perturbation of the bed elevation η_1 driven by the evolution of the bifurcation node, for a given value of the scaled aspect ratio $\epsilon = 0.5$. The lower panels focus on the perturbations at the inlet of the branch and show the dependence on the scaled aspect ratio ϵ of (b) the unit discharge q_1^I and the transport capacity q_{s1}^I, and (c) the bed slope S_1^I and the energy slope j_1^I. The vertical dashed lines in the lower panels mark the scaled aspect ratio $\epsilon = 0.5$ adopted in the upper panel, which corresponds to a bifurcation timescale equal to $T_{BIF} = 10^2$. In all panels, perturbations are divided by the perturbation of the inlet bed elevation η_1^I; both the bed slope and the energy slope are scaled with the corresponding reference values (S_0, j_0).

10969837, 2025, 12, Downloaded from https://onlinelibrary.wiley.com/doi/10.1002/esp.70159 by University Modena, Wiley Online Library on [03/11/2025]. See the Terms and Conditions (https://onlinelibrary.wiley.com/terms-and-conditions) on Wiley Online Library for rules of use; OA articles are governed by the applicable Creative Commons License

the nondominant, aggrading channel becomes steeper at the entrance. As the scaled aspect ratio ϵ vanishes the inlet bed slope is unperturbed, and the flow is locally uniform (i.e., the bed slope equals the energy slope, Figure 9c). This behaviour can be explained by recalling that in the limit $\Omega \to 0$ the length of influence Λ tends to infinity (Figure 7). As a result, any perturbation of the bed elevation propagates along the branch without showing any spatial variability. In this case, the solution coincides with that predicted by Miori et al. (2006b).

5 | DISCUSSION

5.1 | Bifurcation timescale and flow variability

The results of numerical simulations presented in Section 4 highlight the existence of two distinct phases in the transient behaviour of bifurcations, the first of which mainly concerns the local evolution of the bifurcation node. After the water and sediment partitioning at the node, as well as the bed elevation gap between the branches, have almost reached their equilibrium values, a second, longer phase develops in which the bifurcates adapt their bed slope to the equilibrium value set by the water and sediment discharges supplied by the node. The identification of these two phases and their respective timescales may help to reconcile the seemingly contradictory results of previous investigations, which had suggested that the (overall) evolution of bifurcations could be either very slow (Gao et al., 2024; Kleinhans et al., 2008) or very fast (Bertoldi, 2012).

The timescale of both phases is found to increase with the dimensionless branch length L, the second phase being increasingly longer than the first. When L exceeds a threshold value L_{LB}, the downstream boundary condition no longer affects the adaptation of the water and sediment partitioning, and the evolutionary timescale of the bifurcation node attains a constant value. The analysis of the dataset of bifurcation-confluence units collected by Ragno et al. (2022a, 2022b), which encompasses more than 60 gravel-bed bifurcations covering a relatively wide range of hydraulic conditions, suggests that this asymptotic condition is hardly met in real-world bifurcations. Their observed average lengths range between $10^2 - 10^3$ times the mean flow depth (Ragno et al., 2022a, 2022b), while the resulting values of L_{LB} are in the range $10^3 - 10^4$.

In Figure 10 we report the dimensional value of the timescale T^*_{BIF} for all the gravel-bed bifurcations included in the dataset. The resulting values span from about 1 h up to several years, with a median value of 129 h. Our results clearly show that T^*_{BIF} decreases with the reference bed slope S_0; moreover, larger values of T^*_{BIF} are typically associated with wider channels. These trends can be explained by recalling that, according to Equation (1), we scaled the time variable with the Exner timescale T^*_E (defined in Equation 2), which depends primarily on both W^*_0 and S_0. In fact, T^*_E increases linearly with W^*_0, while increasing S_0 gives higher values of the unit transport capacity q^*_{s0} due to the increase in the reference Shields stress.

We note that the typical duration of floods in gravel-bed rivers is much shorter than the values of T^*_{BIF} we estimated, being in the order of several hours. This result implies that single flood events might be unable to produce significant morphological changes at the bifurcation node. Therefore, the long-term response of bifurcations is likely to depend on the average features of the flow regime rather than on the specific sequence of flood events, with different magnitude and duration. In this case, the effect of flow variability on bifurcations can be modelled following an approach similar to that adopted by Carlin et al. (2021) for river bars.

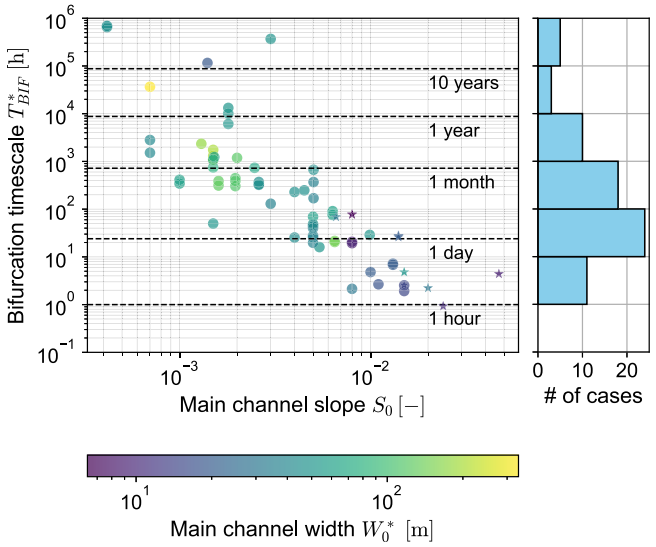

FIGURE 10 Timescale of the gravel-bed river bifurcations included in the dataset by Ragno et al. (2022a, 2022b), computed by means of the linear analysis as a function of the upstream channel slope S_0. The colour scale indicates the upstream channel width W^*_0. Star markers denote bifurcations with "long" branches (i.e., with $L > L_{LB}$).

On the other hand, a different response might be displayed by bifurcations in which the timescale is comparable to that of flow variability. This is the case, for instance, of the gravel-bed bifurcations of the Ridanna Creek and of the Sunwapta River analysed by Zolezzi et al. (2006), which are characterized by a strongly daily signal due to glacier melt during summer. The bankfull geometry of the six bifurcations analysed by the authors is described in Table 1. They are characterized by a bankfull discharge Q^*_0 in the range [4.5,24.7] m^3/s, while they show similar values of channel width $W^*_0 \sim 10^1$ m, bed slope $S_0 \sim 10^{-2}$, flow depth $D^*_0 \sim 10^{-1}$ m and median grain size $D_{s50} \sim 10^{-2}$ m. Moreover, the lengths of the bifurcates, which we estimated using figs. 12 and 13 of the original article, are in the order of $L^* \sim 10^2$ m, which corresponds to $L \sim 10^2$ according to the scaling (1). Let aside one bifurcation in the Ridanna Creek, the length of the bifurcates is considerably lower than the "long-branches" threshold L^*_{LB}, suggesting that the characteristic timescales of these bifurcations might be highly influenced by the downstream conditions. After computing the scaled aspect ratio ϵ, for which we obtained values in the range $\epsilon \in [0.05,1]$, we derived the dimensional timescale T^*_{BIF} of each bifurcation using the linear model. The resulting values, reported in Table 1, suggest that the evolutionary timescale of these bifurcations is typically of the order of a day, thus comparable to that of flow variability.

5.2 | Bifurcation timescale and bar evolution

Among the different forcing factors that may affect the evolutionary trajectories of gravel-bed bifurcations, the fluctuations of sediment

10969837, 2025, 12, Downloaded from https://onlinelibrary.wiley.com/doi/10.1002/esp.70159 by University Modena, Wiley Online Library on [03/11/2025]. See the Terms and Conditions (https://onlinelibrary.wiley.com/terms-and-conditions) on Wiley Online Library for rules of use; OA articles are governed by the applicable Creative Commons License

TABLE 1 Bankfull geometry and timescale of different bifurcations in the Ridanna and Sunwapta pro-glacial gravel bed rivers (data from Zolezzi et al., 2006).

	Rid. 1	Rid. 2	Rid. 3	Sunw. 1	Sunw. 2	Sunw. 3
Q_0^* [m^3/s]	24.7	19.5	6.3	10.3	7.5	4.5
W_0^* [m]	17.4	12.9	9.9	11.3	9.9	8
S_0	0.022	0.017	0.011	0.012	0.014	0.01
D_0^* [m]	0.6	0.68	0.45	0.53	0.44	0.38
D_{s50} [m]	0.1	0.08	0.05	0.04	0.04	0.04
L^* [m]	345	298	144	721	–	471
β_0	14.50	9.49	11.00	10.66	11.25	10.53
θ_0	0.075	0.079	0.053	0.088	0.079	0.058
L	575	438	320	1360	–	1239
ϵ	0.94	0.11	0.73	0.05	0.24	0.50
T_{BIF}^* [h]	1.7	17.3	12.6	133.5	–	16.7
L_{LB}^* [m]	450	2076	804	6300	1517	957

supply caused by the migration of bars in the upstream channel play a relevant role (Burge, 2006; Ferguson et al., 1992). The problem has been tackled by Bertoldi et al. (2009), who investigated the role of bar migration on the equilibrium configurations of bifurcations by means of an analytical model and laboratory experiments. While their study focused on the long-term regime configurations arising from the bar-bifurcation interaction, here we analyse this interaction by comparing the timescales of the two processes.

According to Colombini et al. (1987), the formation of migrating bars and their morphometric properties are mainly controlled by the reference aspect ratio β_0. Specifically, bars form when β_0 exceeds a threshold value β_c, which depends on the reference Shields stress and grain roughness. This critical threshold is typically lower than the resonant value β_R (Seminara & Tubino, 1992), which corresponds to the critical threshold for the bifurcation stability. When $\beta_0 > \beta_c$, alternate bars form and migrate downstream with a given celerity, the inverse of which is employed in the following to estimate the timescale T_{BAR} of migrating bars. Moreover, the bar amplitude increases with β_0, slowing down the bar migration (Colombini et al., 1987). As β_0 exceeds a second threshold β_{NM}, this effect leads the bars to stop migrating.

The three threshold values β_c,β_R, and β_{NM} define the four regions in the (β_0, θ_0) space depicted in Figure 11, each of which identifies a different scenario of interaction between migrating bars and bifurcations. When $\beta_0 < \beta_c$ migrating bars do not form, and balanced bifurcations are stable. If $\beta_0 \in [\beta_c, \beta_R]$, the flow partitioning at bifurcations is likely to oscillate around an even configuration due to the influence of migrating bars that form in the upstream channel.

Let us now focus on the region $\beta_R < \beta_0 < \beta_{NM}$, in which both T_{BAR} and T_{BIF} are positive, and therefore bars interact with bifurcations evolving towards unbalanced equilibrium states. We first note that the timescales of bifurcation evolution and bar migration both depend on the aspect ratio β_0, but show different trends as β_0 increases. On the one hand, T_{BAR} increases monotonically with β_0, and goes to infinity as $\beta_0 \to \beta_{NM}$. On the other hand, $T_{BIF} \to \infty$ for $\beta_0 \to \beta_R$ and then decreases with β_0. As a result, the timescale ratio T_{BAR}/T_{BIF} vanishes as $\beta_0 \to \beta_R$ and goes to infinity as $\beta_0 \to \beta_{NM}$. Between these two

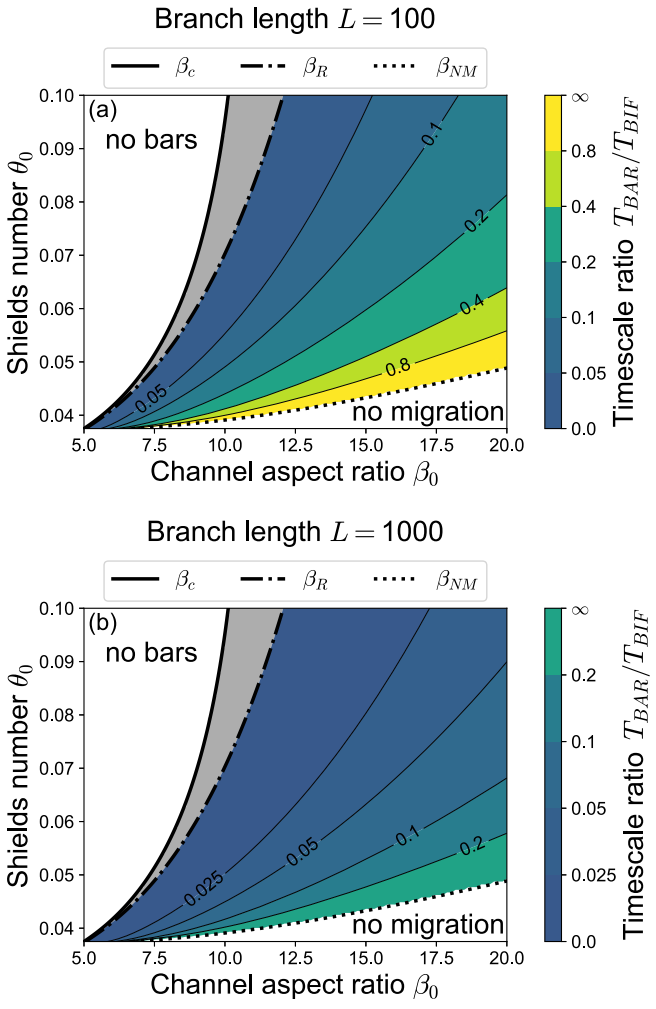

FIGURE 11 Comparison between the bifurcation timescale T_{BIF} and the timescale of bar migration T_{BAR} for different values of the reference aspect ratio β_0 and Shields stress θ_0 and for two values of the branch length L. The solid black lines indicate the critical condition for the formation of migrating bars (β_c), the dash-dotted lines indicate the critical threshold for bifurcation instability (β_R), and the dotted line is the threshold above which bars do no longer migrate (β_{NM}). The gray area between β_c and β_R corresponds to the region where migrating bars coexist with stable, balanced bifurcations.

10969837, 2025, 12, Downloaded from https://onlinelibrary.wiley.com/doi/10.1002/esp.70159 by University Modena, Wiley Online Library on [03/11/2025]. See the Terms and Conditions (https://onlinelibrary.wiley.com/terms-and-conditions) on Wiley Online Library for rules of use; OA articles are governed by the applicable Creative Commons License

thresholds, the timescale ratio increases monotonically with β_0 for a given value of the Shields stress θ_0.

The value of the timescale ratio is also affected by the length of the bifurcates L, which controls the bifurcation timescale T_{BIF} as described in Figure 4. However, changing L does not affect either the threshold values β_c,β_R and β_{NM} or the qualitative trend of T_{BAR}/T_{BIF} across the (β_0, θ_0) space. The role of the branch length emerges clearly when comparing the two panels of Figure 11, which show that by increasing L from 10^2 to 10^3 the ratio T_{BAR}/T_{BIF} decreases by nearly four times. However, even for relatively short branches, the timescale ratio remains smaller than 1 throughout the (β_0, θ_0) phase space, except in the region very close to the threshold of no migration β_{NM}, where the ratio tends to infinity. These results suggest that, generally speaking, the adaptation of the water and sediment partitioning at the bifurcation node is slower compared to bar migration. Similarly to the effect of flow variability on bifurcations, when $T_{BAR}/T_{BIF} \ll 1$ the bifurcation evolution is likely to be determined by the time-averaged amplitude and migration speed of bars. On the other hand, when the two timescales are closer, bifurcations can adapt more quickly to the morphological changes induced at the bifurcation node by bars, so that the flow partitioning closely follows the fluctuations in the water and sediment supply caused by bar migration.

Interestingly, the different areas of the (β_0, θ_0) space shown in Figure 11 are qualitatively similar to the regions of the same phase space identified by Bertoldi et al. (2009) to distinguish the different types of regime conditions arising from the interaction between migrating bars and bifurcations. Firstly, when $\beta_0 < \beta_c$ migrating bars do not form and bifurcations maintain balanced configurations. Next, when β_0 lies between β_c and β_R, migrating bars might produce periodic oscillations around the stable, balanced solution of the bifurcation, as in the "balanced" regime defined by Bertoldi et al. (2009). In the region $\beta_0 > \beta_R$, migrating bars form and interact with evolving bifurcations, which are expected to develop long-term unbalanced configurations. In this case the behaviour of the system depends primarily on the magnitude of T_{BAR}/T_{BIF}. Specifically, for low values of this ratio, the "bar-dominated" behaviour likely prevails; in this regime, migrating bars cause the discharge asymmetry to oscillate around a balanced configuration, even though the intrinsic instability of the bifurcation would produce unbalanced configurations. Increasing the value of T_{BAR}/T_{BIF}, the bifurcation instability becomes dominant, possibly leading to the "bar-perturbed" scenario, in which one branch dominates and migrating bars only produce small oscillations around an unbalanced state.

It is worth highlighting that the interaction between bars and bifurcations does not merely depend on the characteristic timescales, but it is also controlled by the strength of the perturbation exerted by bars, that is, by the bar amplitude. This effect was considered in the theoretical model of Bertoldi et al. (2009), which, however, did not spatially and temporally resolve the evolution of the downstream branches, and therefore could not account for the dependence of T_{BAR}/T_{BIF} on the branch length L. Further insight could be gained by coupling our unsteady model for the bifurcation and the downstream branches with nonlinear bar theories. We also note that different factors can slow down migrating bars in natural rivers, such as curvature (Tubino & Seminara, 1990) and grain sorting effects (Lanzoni & Tubino, 1999), as well as the presence of the steady bar that forms upstream super-resonant bifurcations. The latter problem could be investigated by employing a fully two-dimensional model, such as that proposed by Redolfi et al. (2016).

5.3 | Comparison between different models

Our analysis allows us to clarify the limits of validity of various approximate models that have been proposed so far to analyse the morphodynamic evolution of bifurcates. The comparison between the dependence of the evolutionary timescale of the bifurcation node T_{BIF} on the branch length, as predicted by different models, is presented in Figure 12.

The "long-branches" approximation corresponds to the asymptotic solution of our linear model for $L \to \infty$. In this case, the solution is simply given by the sum of a spatially decaying solution (associated with the positive eigenvalue λ_3) and a "uniform" perturbation (related to the null eigenvalue λ_1), because the influence of the downstream boundary condition is not felt by the evolving node. This approximation clearly returns a length-independent timescale that matches the asymptotic trend of the linear model when L is greater than the threshold value L_{LB}.

The "diffusive" approximation has been widely used in landscape evolution models, and was adopted by Salter et al. (2018) for modelling the morphodynamics of deltaic bifurcations. The solution is obtained by assuming a locally-uniform flow, which is justified when slope variations are so gentle that backwater effects are no longer relevant, so that flow conditions can be determined by considering the bed slope as a proxy for the energy slope. Therefore, the difference between the complete model and the diffusive approximation decreases as L increases, though never vanishes (Figure 12). As shown in Figure 7, the diffusive solution matches that of the complete model as $\Omega \to 0$, that is, as the lengths of influence go to infinity.

The "single-cell" model was used by Bolla Pittaluga et al. (2003) to analyse the stability of the equilibrium solutions. It is based on modelling each downstream channel as a computational cell, characterized by single values of bed slope, water depth, and flow velocity. The flow is assumed to be locally uniform, as in the diffusive model, and the channel slope is to be constant along the branches, so that spatial variations are ignored. In this scheme, the output fluxes at the downstream end are given by the sediment transport capacity, while the sediment input in the branches is set by the BRT nodal point relation. Since this model considers the evolution of each bifurcate as a whole towards its long-term equilibrium, rather than the local evolution at the bifurcation node, it returns a longer timescale than that computed using our complete model for large values of the branch length (Figure 12). For bifurcations with short bifurcates, the single-cell model returns slightly smaller values than our model, due to the lack of spatial variability in its formulation, which prevents it from capturing the negative feedback exerted by the inlet bed slopes of the bifurcates.

A different approximation was introduced by Miori et al. (2006b) in their unsteady model of an evolving bifurcation, which was based on a "local" approach and assumed a constant ratio between the inlet bed slopes of the bifurcates. Like the "single-cell" model, this model does not account for spatial variations, thus neglecting the evolution of the inlet bed slopes and the related negative feedback. Moreover, the solution is given by a perturbation of the uniform flow with a fixed

10969837, 2025, 12, Downloaded from https://onlinelibrary.wiley.com/doi/10.1002/esp.70159 by University Modena, Wiley Online Library on [03/11/2025]. See the Terms and Conditions (https://onlinelibrary.wiley.com/terms-and-conditions) on Wiley Online Library for rules of use; OA articles are governed by the applicable Creative Commons License

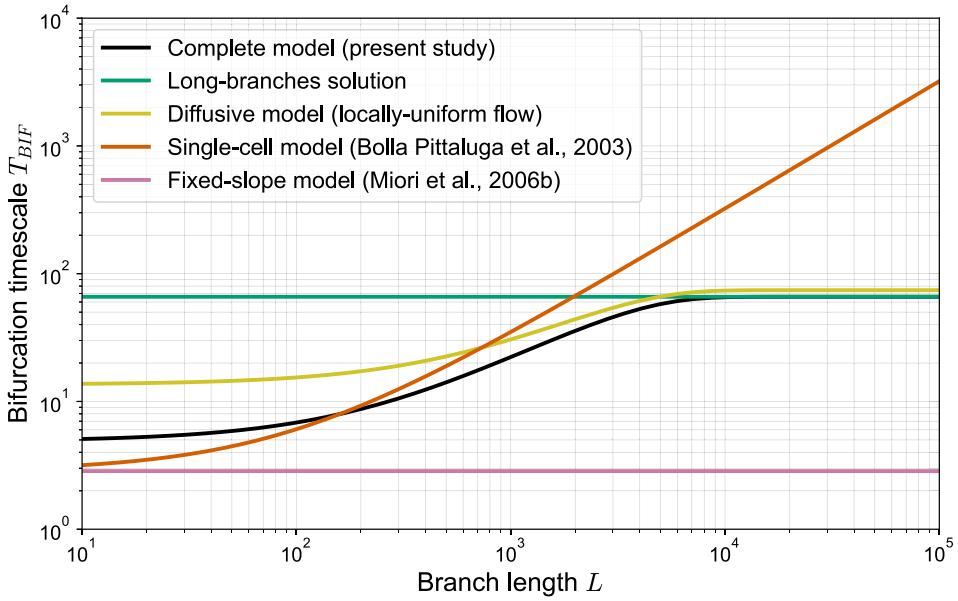

FIGURE 12 Timescale of bifurcation evolution as a function of the branch length L, considering different approaches for modelling the response of the downstream branches. The scaled aspect ratio adopted for all models equals $\epsilon = 1.67$.

slope. The resulting timescale does not depend on the branch length, due to the local nature of the analysis. Consequently, the computed value is lower than that given by our linear solution and corresponds to that of Bolla Pittaluga et al. (2003) in the limiting case $L \to 0$, as shown in Figure 12.

6 | CONCLUSIONS

In this work, we investigated the transient behaviour of river bifurcations by means of an unsteady one-dimensional morphodynamic model, in which the partitioning of water and sediment is described using the nodal point relation of Bolla Pittaluga et al. (2003). We solved the governing equations using both the numerical scheme recently proposed by Barile et al. (2024) and a novel linear analysis, in which we coupled the nodal point relation with a spatially and temporally varying solution for the downstream branches. The results obtained by means of this simplified modelling framework allow us to draw the following general conclusions. First, the water and sediment partition at the bifurcation node evolves on a much shorter timescale than that taken by the bifurcates to reach their long-term equilibrium bed slope. As the flux partitioning asymmetry develops, an erosional and a depositional front form at the upstream end of the branches, affecting the inlet bed slopes, as observed in several field and laboratory investigations on evolving bifurcations. Moreover, our study shows that the evolutionary timescale of the bifurcation node, once scaled with the timescale of bed evolution set by the Exner equation, decreases as the half-width to depth ratio increases above the critical threshold for the bifurcation stability, while it increases with the length of the bifurcates. The latter dependence is due to the condition of constant water level set at the downstream boundary, which speeds up the evolution of the bifurcation node when the length of the bifurcates is small. This accelerating effect vanishes as the branch length exceeds a threshold value, above which the bifurcation timescale no longer depends on the branch length. The threshold value, which can be predicted by means of the linear model, is found to be larger than the observed values of branch length in most natural gravel-bed bifurcations, suggesting that downstream conditions often play a role in their evolutionary process. The values of the bifurcation timescale predicted for real-world gravel-bed bifurcations span from approximately an hour for relatively narrow and steep reaches to several years for wide and mild-sloping channels, with a median value of about a week. Hence, the rate of change in the partitioning of water and sediments at bifurcations is typically much slower than the flow variations associated with the hydrological regime, especially for wide channels. Lastly, our linear analyses suggest that the evolutionary process of bifurcations is typically slower than the migration of alternate bars. However, shorter bifurcates and lower values of the Shields stress of the upstream channel may lead the two processes to evolve on similar timescales.

ACKNOWLEDGEMENTS

The authors have nothing to report. Open access publishing facilitated by Universita degli Studi di Trento, as part of the Wiley - CRUI-CARE agreement.

CONFLICT OF INTEREST STATEMENT

The authors declare that they have no conflict of interest.

DATA AVAILABILITY STATEMENT

The code of the linear model is available at Redolfi (2025). The code used for the numerical model is available at Barile (2023). The dataset of the bankfull geometry of the bifurcation–confluence units is available at Ragno et al. (2022a, 2022b).

ORCID

Gabriele Barile https://orcid.org/0000-0001-7872-4162

REFERENCES

Ashworth, P.J., Best, J.L. & Jones, M. (2004) Relationship between sediment supply and avulsion frequency in braided rivers. *Geology*, 32(1), 21. Available from: https://doi.org/10.1130/G19919.1

10969837, 2025, 12, Downloaded from https://onlinelibrary.wiley.com/doi/10.1002/esp.70159 by University Modena, Wiley Online Library on [03/11/2025]. See the Terms and Conditions (https://onlinelibrary.wiley.com/terms-and-conditions) on Wiley Online Library for rules of use; OA articles are governed by the applicable Creative Commons License

Baar, A.W., de Smit, J., Uijttewaal, W.S.J. & Kleinhans, M.G. (2018) Sediment transport of fine sand to fine gravel on transverse bed slopes in rotating annular flume experiments. *Water Resources Research*, 54(1), 19–45. Available from: https://doi.org/10.1002/2017WR020604

Barile, G. (2023) A python 1d numerical model of a river bifurcation. Zenodo [code]. https://doi.org/10.5281/zenodo.10079752

Barile, G., Redolfi, M. & Tubino, M. (2024) Analysis of autogenic bifurcation processes resulting in river avulsion. *Earth Surface Dynamics*, 12(1), 87–103. Available from: https://doi.org/10.5194/esurf-12-87-2024

Bertoldi, W. (2012) Life of a bifurcation in a gravel-bed braided river. *Earth Surface Processes and Landforms*, 37(12), 1327–1336. Available from: https://doi.org/10.1002/esp.3279

Bertoldi, W. & Tubino, M. (2007) River bifurcations: experimental observations on equilibrium configurations. *Water Resources Research*, 43(10), 1–10. Available from: https://doi.org/10.1029/2007WR005907

Bertoldi, W., Zanoni, L., Miori, S., Repetto, R. & Tubino, M. (2009) Interaction between migrating bars and bifurcations in gravel bed rivers. *Water Resources Research*, 45(6), 1–12. Available from: https://doi.org/10.1029/2008WR007086

Bogoni, M., Putti, M. & Lanzoni, S. (2017) Modeling meander morphodynamics over self-formed heterogeneous floodplains. *Water Resources Research*, 53(6), 5137–5157. Available from: https://doi.org/10.1002/2017WR020726

Bolla Pittaluga, M., Coco, G. & Kleinhans, M.G. (2015) A unified framework for stability of channel bifurcations in gravel and sand fluvial systems. *Geophysical Research Letters*, 42(18), 7521–7536. Available from: https://doi.org/10.1002/2015GL065175

Bolla Pittaluga, M., Repetto, R. & Tubino, M. (2003) Channel bifurcation in braided rivers: equilibrium configurations and stability. *Water Resources Research*, 39(3), 1–13. Available from: https://doi.org/10.1029/2001WR001112

Brooke, S., Chadwick, A.J., Silvestre, J., Lamb, M.P., Edmonds, D.A. & Ganti, V. (2022) Where rivers jump course. *Science*, 376(6596), 987–990. Available from: https://doi.org/10.1126/science.abm1215

Burge, L.M. (2006) Stability, morphology and surface grain size patterns of channel bifurcation in gravel–cobble bedded anabranching rivers. *Earth Surface Processes and Landforms*, 31(10), 1211–1226. Available from: https://doi.org/10.1002/esp.1325

Camporeale, C., Perona, P., Porporato, A. & Ridolfi, L. (2007) Hierarchy of models for meandering rivers and related morphodynamic processes. *Reviews of Geophysics*, 45(1), 1–28. Available from: https://doi.org/10.1029/2005RG000185

Carlin, M., Redolfi, M. & Tubino, M. (2021) The long-term response of alternate bars to the hydrological regime. *Water Resources Research*, 57(7), e2020WR029314. Available from: https://doi.org/10.1029/2020WR029314

Chadwick, A.J., Lamb, M.P. & Ganti, V. (2020) Accelerated river avulsion frequency on lowland deltas due to sea-level rise. *Proceedings of the National Academy of Sciences*, 117(30), 17584–17590. Available from: https://doi.org/10.1073/pnas.1912351117

Colombini, M., Seminara, G. & Tubino, M. (1987) Finite-amplitude alternate bars. *Journal of Fluid Mechanics*, 181(1), 213–232. Available from: https://doi.org/10.1017/S0022112087002064

Durante, L., Bolla Pittaluga, M., Porcile, G. & Tambroni, N. (2024) Downstream control on the stability of river bifurcations. *Journal of Geophysical Research: Earth Surface*, 129(10), e2023JF007548. Available from: https://doi.org/10.1029/2023JF007548

Edmonds, D.A. & Slingerland, R.L. (2008) Stability of delta distributary networks and their bifurcations. *Water Resources Research*, 44(9), 9426. Available from: https://doi.org/10.1029/2008WR006992

Eke, E.C., Czapiga, M.J., Viparelli, E., Shimizu, Y., Imran, J., Sun, T., et al. (2014) Coevolution of width and sinuosity in meandering rivers. *Journal of Fluid Mechanics*, 760, 127–174. Available from: https://doi.org/10.1017/jfm.2014.556

Fasolato, G., Ronco, P. & Silvio, G.D. (2009) How fast and how far do variable boundary conditions affect river morphodynamics? *Journal of Hydraulic Research*, 47(3), 329–339. Available from: https://doi.org/10.3826/jhr.2009.3338

Ferguson, R.I. (1993) Understanding braiding processes in gravel-bed rivers: progress and unsolved problems. *Geological Society, London, Special Publications*, 75(1), 73–87. Available from: https://doi.org/10.1144/GSL.SP.1993.075.01.03

Ferguson, R.I., Ashmore, P.E., Ashworth, P.J., Paola, C. & Prestegaard, K.L. (1992) Measurements in a braided river chute and lobe: 1. Flow pattern, sediment transport, and channel change. *Water Resources Research*, 28(7), 1877–1886. Available from: https://doi.org/10.1029/92WR00700

Gao, W., Shao, D., Wang, Z.B., Zhu, Z. & Yang, Z. (2024) System-wide effects of local bed disturbance on the morphological evolution of a bifurcating channel network. *Journal of Geophysical Research - Earth Surface*, 129(3), e2023JF007514. Available from: https://doi.org/10.1029/2023JF007514

Jerolmack, D.J. & Mohrig, D. (2007) Conditions for branching in depositional rives. *Geology*, 35(5), 463–466. Available from: https://doi.org/10.1130/G23308A.1

Kleinhans, M.G., Ferguson, R., Lane, S.N. & Hardy, R.J. (2013) Splitting rivers at their seams: bifurcations and avulsion. *Earth Surface Processes and Landforms*, 38(1), 47–61. Available from: https://doi.org/10.1002/esp.3268

Kleinhans, M.G., Jagers, H.R., Mosselman, E. & Sloff, C.J. (2008) Bifurcation dynamics and avulsion duration in meandering rivers by one-dimensional and three-dimensional models. *Water Resources Research*, 44(8), 2007WR005912. Available from: https://doi.org/10.1029/2007WR005912

Lanzoni, S. & Tubino, M. (1999) Grain sorting and bar instability. *Journal of Fluid Mechanics*, 393, 149–174. Available from: https://doi.org/10.1017/S0022112099005583

Le, T.B., Crosato, A., Mosselman, E. & Uijttewaal, W.S. (2018) On the stability of river bifurcations created by longitudinal training walls. Numerical investigation. *Advances in Water Resources*, 113(July 2017), 112–125. Available from: https://doi.org/10.1016/j.advwatres.2018.01.012

Leddy, J.O., Ashworth, P.J. & Best, J.L. (1993) Mechanisms of anabranch avulsion within gravel-bed braided rivers: observations from a scaled physical model. *Geological Society, London, Special Publications*, 75(1), 119–127. Available from: https://doi.org/10.1144/GSL.SP.1993.075.01.07

Liang, M., Van Dyk, C. & Passalacqua, P. (2016) Quantifying the patterns and dynamics of river deltas under conditions of steady forcing and relative sea level rise. *Journal of Geophysical Research: Earth Surface*, 121(2), 465–496. Available from: https://doi.org/10.1002/2015JF003653

Mendoza, A., Berezowsky, M., Caballero, C. & Arganis-Juárez, M. (2022) Alteration of the flow distribution at a river bifurcation caused by a system of upstream dams: case of the Grijalva River basin, Mexico. *Earth Surface Processes and Landforms*, 47(2), 509–521. Available from: https://doi.org/10.1002/esp.5265

Miori, S., Repetto, R. & Tubino, M. (2006a) Unsteadiness effects on the morphological behaviour of gravel-bed river bifurcations. In: Alves, E., Cardoso, A., Leal, J. & Ferreira, R. (Eds.) *River flow 2006*. London: Taylor & Francis. Available from: https://doi.org/10.1201/9781439833865.ch136

Miori, S., Repetto, R. & Tubino, M. (2006b) A one-dimensional model of bifurcations in gravel bed channels with erodible banks. *Water Resources Research*, 42(11), 1–12. Available from: https://doi.org/10.1029/2006WR004863

Monegaglia, F. & Tubino, M. (2019) The hydraulic geometry of evolving meandering rivers. *Journal of Geophysical Research: Earth Surface*, 124(11), 2723–2748. Available from: https://doi.org/10.1029/2019JF005309

Monegaglia, F., Tubino, M. & Zolezzi, G. (2019) Interaction between curvature-driven width oscillations and channel curvature in evolving meander bends. *Journal of Fluid Mechanics*, 876, 985–1017. Available from: https://doi.org/10.1017/jfm.2019.574

Parker, G. (1978) Self-formed straight rivers with equilibrium banks and mobile bed. Part 2. The gravel river. *Journal of Fluid Mechanics*, 89(1), 127–146. Available from: https://doi.org/10.1017/S0022112078002505

10969837, 2025, 12, Downloaded from https://onlinelibrary.wiley.com/doi/10.1002/esp.70159 by University Modena, Wiley Online Library on [03/11/2025]. See the Terms and Conditions (https://onlinelibrary.wiley.com/terms-and-conditions) on Wiley Online Library for rules of use; OA articles are governed by the applicable Creative Commons License

Parker, G., Shimizu, Y., Wilkerson, G.V., Eke, E.C., Abad, J.D., Lauer, J.W., et al. (2011) A new framework for modeling the migration of meandering rivers. *Earth Surface Processes and Landforms*, 36(1), 70–86. Available from: https://doi.org/10.1002/esp.2113

Ragno, N., Redolfi, M. & Tubino, M. (2021) Coupled morphodynamics of river bifurcations and confluences. *Water Resources Research*, 57(1), e2020WR028515. Available from: https://doi.org/10.1029/2020WR028515

Ragno, N., Redolfi, M. & Tubino, M. (2022a) Quasi-universal length scale of river anabranches. *Geophysical Research Letters*, 49(16), e2022GL099928. Available from: https://doi.org/10.1029/2022GL099928

Ragno, N., Redolfi, M. & Tubino, M. (2022b) Loops length data (Version 1.0.0). Zenodo. https://doi.org/10.5281/zenodo.6901398

Ragno, N., Tambroni, N. & Bolla Pittaluga, M. (2020) Effect of small tidal fluctuations on the stability and equilibrium configurations of bifurcations. *Journal of Geophysical Research: Earth Surface*, 125(8), 1–20. Available from: https://doi.org/10.1029/2020JF005584

Redolfi, M. (2021) Free alternate bars in rivers: key physical mechanisms and simple formation criterion. *Water Resources Research*, 57(12), e2021WR030617. Available from: https://doi.org/10.1029/2021wr030617

Redolfi, M. (2023) Defining the length parameter in river bifurcation models: a theoretical approach. *Earth Surface Processes and Landforms*, 48(11), 2121–2132. Available from: https://doi.org/10.1002/esp.5673

Redolfi, M. (2025). Unsteady linear analysis of the 1-D morphodynamic model for river bifurcations. Zenodo [code]. Available from: https://doi.org/10.5281/zenodo.17097434

Redolfi, M., Zolezzi, G. & Tubino, M. (2016) Free instability of channel bifurcations and morphodynamic influence. *Journal of Fluid Mechanics*, 799, 476–504. Available from: https://doi.org/10.1017/jfm.2016.389

Redolfi, M., Zolezzi, G. & Tubino, M. (2019) Free and forced morphodynamics of river bifurcations. *Earth Surface Processes and Landforms*, 44(4), 973–987. Available from: https://doi.org/10.1002/esp.4561

Riquier, J., Piégay, H. & Šulc Michalková, M. (2015) Hydromorphological conditions in eighteen restored floodplain channels of a large river: linking patterns to processes. *Freshwater Biology*, 60(6), 1085–1103. Available from: https://doi.org/10.1111/fwb.12411

Salter, G., Paola, C. & Voller, V.R. (2018) Control of delta avulsion by downstream sediment sinks. *Journal of Geophysical Research: Earth Surface*, 123(1), 142–166. Available from: https://doi.org/10.1002/2017JF004350

Seminara, G. (2010) Fluvial sedimentary patterns. *Annual Review of Fluid Mechanics*, 42(1), 43–66. Available from: https://doi.org/10.1146/annurev-fluid-121108-145612

Seminara, G. & Tubino, M. (1992) Weakly nonlinear theory of regular meanders. *Journal of Fluid Mechanics*, 244(1), 257–288. Available from: https://doi.org/10.1017/S0022112092003069

Seminara, G., Zolezzi, G., Tubino, M. & Zardi, D. (2001) Downstream and upstream influence in river meandering. Part 2. Planimetric development. *Journal of Fluid Mechanics*, 438, 213–230. Available from: https://doi.org/10.1017/S0022112001004281

Struiksma, N., Olesen, K., Flokstra, C. & De Vriend, H.J. (1985) Bed deformation in curved alluvial channels. *Journal of Hydraulic Research*, 23(1), 57–79. Available from: https://doi.org/10.1080/00221688509499377

Szewczyk, L., Grimaud, J.-L. & Cojan, I. (2020) Experimental evidence for bifurcation angles control on abandoned channel fill geometry. *Earth Surface Dynamics*, 8(2), 275–288. Available from: https://doi.org/10.5194/esurf-8-275-2020

Szewczyk, L., Grimaud, J.-L., Cojan, I. & Piegay, H. (2022) Bedload infilling and depositional patterns in chute cutoffs channels of a gravel-bed river: the Ain River, France. *Earth Surface Processes and Landforms*, 47(2), 459–476. Available from: https://doi.org/10.1002/esp.5260

Toonen, W.H.J., Kleinhans, M.G. & Cohen, K.M. (2012) Sedimentary architecture of abandoned channel fills. *Earth Surface Processes and Landforms*, 37(4), 459–472. Available from: https://doi.org/10.1002/esp.3189

Tubino, M. (1991) Growth of alternate bars in unsteady flow. *Water Resources Research*, 27(1), 37–52. Available from: https://doi.org/10.1029/90WR01699

Tubino, M. & Seminara, G. (1990) Free–forced interactions in developing meanders and suppression of free bars. *Journal of Fluid Mechanics*, 214, 131–159. Available from: https://doi.org/10.1017/S0022112090000088

Van Denderen, R.P., Schielen, R.M., Blom, A., Hulscher, S.J.M.H. & Kleinhans, M.G. (2018) Morphodynamic assessment of side channel systems using a simple one-dimensional bifurcation model and a comparison with aerial images. *Earth Surface Processes and Landforms*, 43(6), 1169–1182. Available from: https://doi.org/10.1002/esp.4267

Van Denderen, R.P., Schielen, R.M., Westerhof, S.G., Quartel, S. & Hulscher, S.J. (2019) Explaining artificial side channel dynamics using data analysis and model calculations. *Geomorphology*, 327, 93–110. Available from: https://doi.org/10.1016/j.geomorph.2018.10.016

Wagner, W. & Mohrig, D. (2019) Flow and sediment flux asymmetry in a branching channel delta. *Water Resources Research*, 55(11), 9563–9577. Available from: https://doi.org/10.1029/2019WR026050

Wong, M. & Parker, G. (2006) One-dimensional modeling of bed evolution in a gravel bed river subject to a cycled flood hydrograph. *Journal of Geophysical Research: Earth Surface*, 111(F3), 2006JF000478. Available from: https://doi.org/10.1029/2006JF000478

Zolezzi, G., Bertoldi, W. & Tubino, M. (2006) Morphological analysis and prediction of river bifurcations. In: *Braided Rivers*. Oxford: Blackwell Publishing Ltd, pp. 233–256 https://doi.org/10.1002/9781444304374.ch11

Zolezzi, G. & Seminara, G. (2001) Downstream and upstream influence in river meandering. Part 1. General theory and application to overdeepening. *Journal of Fluid Mechanics*, 438(July), 183–211. Available from: https://doi.org/10.1017/S002211200100427X

SUPPORTING INFORMATION

Additional supporting information can be found online in the Supporting Information section at the end of this article.

How to cite this article: Barile, G., Redolfi, M. & Tubino, M. (2025) Time scales of river bifurcations. *Earth Surface Processes and Landforms*, 50(12), e70159. Available from: https://doi.org/10.1002/esp.70159

10969837, 2025, 12, Downloaded from https://onlinelibrary.wiley.com/doi/10.1002/esp.70159 by University Modena, Wiley Online Library on [03/11/2025]. See the Terms and Conditions (https://onlinelibrary.wiley.com/terms-and-conditions) on Wiley Online Library for rules of use; OA articles are governed by the applicable Creative Commons License